Regime dependence of Aerosol Effects on the Formation and Evolution of Pyro-convective clouds

Di Chang[1], Yafang Cheng[1], Philipp Reutter[2], Jörg Trentmann[3], Susannah Burrows[4], Peter Spichtinger[2], Stephan Nordmann[1], Meinrat O. Andreae[5], Ulrich Pöschl[1], and Hang Su[1,*]

[1]Multiphase Chemistry Department, Max Planck Institute for Chemistry, Mainz, Germany

[2]Institute for Atmospheric Physics (IPA), Johannes Gutenberg University Mainz, Mainz, Germany

[3]German Weather Service (DWD), Offenbach, Germany

[4]Pacific Northwest National Laboratory, Richland, WA, USA

[5]Biogeochemistry Department, Max Planck Institute for Chemistry, Mainz, Germany

[*]Correspondence to: h.su@mpic.de

Abstract

A recent parcel model study (Reutter et al., 2009) showed three deterministic regimes of initial cloud droplet formation, characterized by different ratios of aerosol concentrations (N_{CN}) to updraft velocities. This analysis, however, did not reveal how these regimes evolve during the subsequent cloud development. To address this issue, we employed the Active Tracer High Resolution Atmospheric Model (ATHAM) with full microphysics and extended the model simulation from the cloud base to the entire column of a single pyro-convective mixed-phase cloud. A series of 2-D simulations (over 1000) were performed over a wide range of N_{CN} and dynamic conditions. The integrated concentration of hydrometeors over the full spatial and temporal scales was used to evaluate the aerosol and dynamic effects. The results show that: (1) the three regimes for cloud condensation nuclei (CCN) activation in the parcel model (namely aerosol-limited, updraft-limited, and transitional regimes) still exist within our simulations, but net production of raindrops and frozen particles occurs mostly within the updraft-limited regime. (2) Generally, elevated aerosols enhance the formation of cloud droplets and frozen particles. The response of raindrops and precipitation to aerosols is more complex and can be either positive or negative as a function of aerosol concentrations. The most negative effect was found for values of N_{CN} of ~1000 to 3000 cm^{-3}. (3) The nonlinear properties of aerosol-cloud interactions challenge the conclusions drawn from limited case studies in terms of their representativeness, and ensemble studies over a wide range of aerosol concentrations and other influencing factors are strongly recommended for a more robust assessment of the aerosol effects.

Keywords: pyro-convective clouds, precipitation, ATHAM, updrafts, aerosol

1. Introduction

Clouds have a considerable impact on the radiation budget and water cycle of the Earth (IPCC, 2007). Aerosol effects on clouds and precipitation have been suggested to influence the formation, persistence, and ultimate dissipation of clouds and its climate effects (Stevens and Feingold, 2009; Tao et al., 2012), and hence have been studied intensively through cloud-resolving model simulations, analysis of satellite data, and long-term observational data (Tao et al., 2012).

However, aerosol effects are still associated with significant uncertainty in light of the seemingly contradictory results from different studies. For instance, several studies have indicated that increasing aerosol concentrations could reduce cloud fraction and inhibit cloud formation (Albrecht, 1989; Ackerman et al., 2000; Kaufman et al., 2002; Koren et al., 2004), whereas it is suggested that more aerosols can increase the cloud fraction in other studies (Norris, 2001; Kaufman and Koren, 2006; Grandey et al., 2013). Precipitation from stratiform clouds can be inhibited by elevated aerosol concentration (Zhang et al., 2006), while precipitation from convective clouds can be either suppressed or enhanced (Ackerman et al., 2003; Andreae et al., 2004; Altaratz et al., 2008; Lee et al., 2008; Teller and Levin, 2008; Fan et al., 2013; Camponogara et al., 2014). In addition, changing aerosol concentrations have also been found to exert non-monotonic influences (either positive or negative) on a wide range of cloud properties, such as homogeneous freezing (Kay and Wood, 2008), frozen water particles (Saleeby et al., 2009; Seifert et al., 2012), and convection strength (Fan et al., 2009).

One explanation for these seemingly contradictory results is that aerosol effects are regime-dependent, which means that it can vary under different meteorological conditions (updraft velocity, relative humidity, surface temperature, and wind shear), cloud types, aerosol properties (size distribution and chemical composition) and observational or analysis scales (Levin and Cotton, 2007; Tao et al., 2007; Khain et al., 2008; Rosenfeld et al., 2008; Fan et al., 2009; Khain, 2009; Reutter et al., 2009; McComiskey and Feingold, 2012; Tao et al., 2012). It is thus important to investigate the regime-dependence of aerosol-cloud interactions and to improve the representation of cloud regimes in models (Stevens and Feingold, 2009). If we were able to distinguish under which conditions cloud formation is updraft-limited (aerosol-insensitive) as discussed in Reutter et al. (2009), it would have the advantage that in future work one could for many purposes neglect aerosol effects on clouds in areas that are usually updraft limited.

Another challenge in evaluating the aerosol effects lies in the nonlinear properties of aerosol-cloud interactions. Most previous research investigated the response of clouds and precipitation to the perturbation of aerosols based on two or several individual scenarios, by doubling or tripling the number concentration of aerosol particles. This will be fine for the linear dependence. Since aerosol-cloud interaction is a nonlinear process, such method may not reflect the real aerosol effect. An exemplary case is shown in Fig. 1, in which it is clear that the local derivatives ($d\mathrm{Y}/d\mathrm{X}$) can be different from $\Delta\mathrm{Y}/\Delta\mathrm{X}$ determined by the difference between A and B cases.

Biomass burning generates significant amounts of smoke aerosols, and the fires loft soil particles that contain minerals (Pruppacher and Klett, 1997), both of which could serve as effective cloud condensation nuclei (CCN) and ice nuclei (IN) (Hobbs and Locatelli, 1969; Hobbs and Radke, 1969; Kaufman and Fraser, 1997; Sassen and Khvorostyanov, 2008), thereby affecting the formation of clouds and precipitation. As an extreme consequence of biomass burning, pyro-clouds feed directly from the smoke and heat released from fires (Andreae et al., 2004; Luderer, 2007) and provide a good example with which to study aerosol-cloud interactions (Reutter et al., 2009).

By taking the pyro-convective clouds as an example, here we demonstrate the ability of ensemble simulations to determine the regime dependence and resolve the nonlinear properties of aerosol-cloud interactions. Aerosol number concentration, updraft velocity (represented by the intensity of fire forcing, which triggers updraft velocities), and key parameters of CCN activation (Reutter et al., 2009) are varied to represent a wide range of aerosol and dynamic conditions. In addition to cloud droplets, the responses of precipitable hydrometeors (raindrops, ice, snow, graupel, and hail) were also investigated. For a better understanding of the mechanisms, we employed the process analysis (PA) method, which documents the rate of change in the mass or number concentration of each hydrometeor type caused by a particular process, thereby enabling the determination of the relative importance of the major microphysical processes under different dynamic forcing and aerosol conditions.

2. Design of numerical experiments

2.1 ATHAM: model and configuration

The Active Tracer High Resolution Atmospheric Model (ATHAM), a non-hydrostatic model, is used here to study cloud formation and evolution in response to changes in updrafts and aerosol particle concentration. ATHAM was designed initially to investigate high-energy plumes in the atmosphere and applied to simulate volcanic eruptions and fire plumes (Herzog, 1998; Oberhuber et al., 1998). ATHAM has been used to simulate the evolution of pyro-cumulonimbus clouds (pyroCb) caused by a forest fire and shows results consistent with observations (Luderer, 2007).

The model comprises eight modules: dynamics, turbulence, cloud microphysics, ash aggregation, gas scavenging, radiation, chemistry, and soil modules (Herzog et al., 1998; Oberhuber et al., 1998; Graf et al., 1999; Herzog et al., 2003). Cloud microphysical interactions are represented by an extended version of the two-moment scheme developed by Seifert and Beheng (2006), which includes the hail modifications by Blahak (2008), and is able to predict the numbers and mass mixing ratios of six classes of hydrometeors (cloud water, ice crystals, raindrops, snow, graupel, and hail; detailed in Table 1) and water vapor. It has been validated successfully against a comprehensive spectral bin microphysics cloud model (Seifert et al., 2006). The cloud nucleation (CCN activation) module is based on a lookup table derived from parcel model simulations for pyro-convective clouds (Reutter et al., 2009). The ATHAM model can execute both 2-D and 3-D simulations. Results of this study are mainly based on 2-D simulations.

The meteorological conditions were set up to simulate the Chisholm forest fire (Luderer, 2007; Rosenfeld et al., 2007), which is a well-documented case of pyro-convection. All simulations were initialized horizontally homogeneously with radiosonde data from about 200 km south of the fire on 29 May 2001, which is the same as in Luderer (2007) (Fig. 2). The vertical profiles of the temperature and dew point temperature reveal a moderate instability in the atmosphere. Open lateral boundaries were used for the model simulations. The means of wind speed and specific humidity were nudged towards the initial profile at the lateral boundaries. The fire forcing was introduced in the middle grid in the bottom layer of the domain, and its intensity remained constant throughout the simulation of each scenario. Each case was run for 3 simulated hours until the clouds were fully developed and had reached steady state.

The 2-D simulations were performed at the cross section of the fire front. The simulation domain was set at 85 × 26 km with 110 × 100 grid boxes in the x and z directions. The horizontal grid box size at the center of the x direction was equal to 500 m, and it enlarged towards the lateral boundaries due to the stretched grid (Fig. 3). Such a process scale with resolution of ca. 1 km has been suggested as the appropriate scale at which to characterize processes related to aerosol-cloud interactions (McComiskey and Feingold, 2012). The vertical grid spacing at the surface and the tropopause was set to 50 and 150 m, respectively. The lowest vertical level in our simulation was placed 766 m above sea level, corresponding to the lowest elevation of the radiosonde data, which is close to the elevation of Chisholm at about 600 m (ASRD, 2001). The results of the 2-D simulations are presented and discussed in Sect. 3.

2.2 Aerosol particles and fire forcing

Atmospheric aerosol particles affect cloud formation through two pathways, by acting as CCN and as IN. Following the previous study of Reutter et al. (2009), we limited the scope of aerosol-cloud interactions to CCN activation only. So, in this study, changes in N_{CN} do not directly influence frozen hydrometeors by providing IN, but do so indirectly through their impact on CCN activation and subsequent processes.

In the 2-D ensemble simulations, 1302 cases (31 N_{CN} × 42 fire forcing values) were simulated to evaluate the interplay of aerosol concentration and updrafts on the formation of clouds and precipitation. The N_{CN} varied from 200 to 100,000 cm^{-3}. In each case, N_{CN} was prescribed (distributed uniformly across the modeling domain and kept identical throughout the simulation). A similar prescribed approach has been used in previous studies (Seifert et al., 2012; Reutter et al., 2014). Some previous studies have pointed out that a prescribed aerosol scheme overestimates the magnitude of CCN concentrations compared to a prognostic aerosol scheme, because it lacks a representation of the efficient removal of particles by nucleation scavenging (Wang et al., 2013).

As mentioned above, we used the lookup table of Reutter et al. (2009) for the CCN activation. This table is determined for fresh biomass burning aerosols with a hygroscopicity parameter κ of 0.2 and a log-normal size distribution (a geometric mean diameter of 120 nm and a geometric standard deviation of 1.5, Reutter et al. 2009). For the present study, the aerosol characteristics, such as size distribution, chemical composition, hygroscopicity and mixing state are in fact rather unimportant, compared with the order-of-magnitude changes in the aerosol number concentration (Reutter et al., 2009; Karydis et al., 2012). Therefore, the effects of variations in aerosol characteristics were not considered in our study.

In all simulations, clouds were triggered by the fire forcing, which was assumed constant during the simulation. The fire forcing intensity varied from 1×10^3 to 3×10^5 W m^{-2}. The correlation between the initial fire forcing and corresponding updraft velocity and temperature at the cloud base was probed and is described in Sect. 3.1.

In reality, the composition and quantity of biomass burning emissions depend on the moisture content of fuels, combustion conditions, weather situation, and fire behavior (Bytnerowicz et al., 2009). What’s more, the biomass burning plumes can in turn change the relative humidity as well. The aerosol particle number concentrations in biomass burning plumes usually exceed 10^4 cm^{-3}, and can be up to ~10^5 cm^{-3} (Andreae et al., 2004; Reid et al., 2005). In contrast to regular convection, the updraft velocities in pyro-convective clouds are normally larger than 20~30 m s^{-1} (Khain et al., 2005). On the basis of these facts, within our work more attention is paid to situations with higher aerosol concentration (>10^4 cm^{-3}) and strong updrafts (>20 m s^{-1}), which are more representative of pyro-convective clouds.

2.3 Process analysis

Cloud properties are subject to several tens of microphysical processes, e.g., cloud droplet nucleation, autoconversion, freezing, condensation, evaporation, etc. (Seifert and Beheng, 2006). Elevated concentrations of hydrometeors can be caused either by an increase in their sources or by a decrease in their sinks. To improve the understanding of the aerosol-cloud interactions, we employed the process analysis (PA) method to quantify the causation of changes in the concentrations of individual hydrometeor classes.

In addition to the standard model output (e.g., time and spatial series of mass and number concentrations of hydrometeors, and meteorological output), our PA method archives additional parameters, i.e., the time rate of change of hydrometeors due to individual microphysical processes under different aerosol and fire forcing conditions. Table A1 summarizes all the microphysical processes and their acronyms.

2.4 3-D simulations

In addition, we performed a number of 3-D simulations to investigate its difference to 2-D simulations. As the 3-D simulations are computationally expensive, only 99 cases (11 $N_{\mathrm{CN}} \times 9$ fire forcing values) were performed. N_{CN} varied from 200 to 100,000 cm^{-3}, while fire forcing varied between 1×10^3 and 8×10^4 W m^{-2}. The size of the model domain was set at $85 \times 65 \times 26$ km with $110 \times 85 \times 100$ grid boxes in the x, y and z directions. For consistency, the grid resolutions in the x and z directions were the same as for 2-D simulations. The minimum grid box size in the y direction was set to 100 m. The results of the 3-D simulations are presented and discussed in supplementary material.

3. Results and discussion

3.1 Relationship between updraft velocity, temperature, and fire forcing

Fire forcing does not affect the cloud activation of aerosols directly, but it can affect activation indirectly by triggering strong updraft velocities. Updrafts are of importance in the formation of clouds and precipitation for redistributing energy and moisture. To cover a wide range of conditions, the updraft velocities range from ca. 0.25 to 20 m s^{-1} in previous cloud parcel model simulations (Reutter et al., 2009), which represent the range found in trade wind cumulus to thunderstorms (Pruppacher and Klett, 1997).

The probability distribution function of vertical velocities (*w*) at cloud base layer under different fire forcing conditions is shown in Fig. 4a. The velocity on top of the input fire forcing is usually the largest, and decreases towards the lateral sides. As the characteristic velocities, the maximum velocity at cloud base in Fig. 4a, are plotted against the input fire forcing (range of 1×10^3 to 3×10^5 W m^{-2}, $N_{CN} = 1 \times 10^3$ cm^{-3}) in Fig. 4b. The shaded area indicates the variability of estimation over each simulation period. According to the figure, *w* at cloud base varies monotonically from 1.8 to 27 m s^{-1} as fire forcing increases from 1×10^3 to 3×10^5 W m^{-2}. The positive relationship suggests that fire forcing could be a good indicator of vertical velocity. Because it is a variable of central interest to the cloud research community, the maximum vertical velocity is provided along with the fire forcing values as an additional axis in the following plots.

Another variable of key meteorological interest is the maximum temperature at cloud base. To clarify how temperature is affected by fire forcing in our simulations, the relationship between fire forcing and the corresponding maximum temperature at cloud base is shown in Fig. 5. As variations in aerosol number concentrations have very little effect on the temperature profile, we show this relationship for only one aerosol concentration (N_{CN}=5,000 cm^{-3}) as an example. Based on Fig. 5, the cloud base temperature increases linearly from 7.6 to 16.4 ℃, as fire forcing is enhanced from 1×10^3 to 3×10^5 W m^{-2}. In order to more clearly convey the effect of the heating imposed in the simulation, we have used this linear relationship to add the maximum cloud base temperature as a secondary axis in the figures.

Finally, we note that the horizontal wind shear can also affect the convection strength (Fan et al., 2009), which could be investigated in detail in future studies.

3.2 Aerosol effects and its regime dependence

In this section, the tempo-spatial distribution of each hydrometeor type will be briefly presented, followed by the modeled dependency of various hydrometeors on N_{CN} and fire forcing (*FF*). Note here only the characteristics of dependency are presented, while the underlying mechanisms will be discussed and interpreted in more detail in Sect. 3.3. For an individual hydrometeor type, the averaged concentrations (over the entire domain and simulation period) were used as metrics in our evaluation, and the condensed water reaching the surface was used as a metric for precipitation.

3.2.1 Cloud droplets

Figure 6 shows the temporal evolution of horizontally-averaged mass concentration of cloud droplets (M_{CD}) under the four pairs of *FF* and N_{CN} conditions. Under weak fire forcing conditions (LU), the formation of cloud droplets usually occurs from 20 min, and concentrates at an altitude of 4-7 km. The duration of cloud droplets usually last for a short period (40~60 min). Under strong fire forcing conditions (HU), the cloud droplets form earlier (around 5 min), and most cloud droplets are located at a height of 5-9 km. Besides, the cloud droplets reach steady state because of the cycling of cloud formation.

To investigate the sensitivity of an individual hydrometeor to changes in N_{CN} and *FF*, we adopted the definition of relative sensitivity $RS_Y(X)$ (of one variable *Y* against the variable *X*) as

$$RS_Y(X) = \frac{\partial Y / Y}{\partial X / X} = \frac{\partial \ln Y}{\partial \ln X} \quad (1)$$

In this study, *X* is the factor affecting cloud formation, i.e., N_{CN} and *FF*, and *Y* is the mass or number concentration of each hydrometeor type (cloud droplets, raindrops, as well as frozen particles). By using a natural logarithmic calculation of the variables (i.e., *X*, *Y*), the percentage change of an individual parameter relative to its magnitude could be reflected better. This logarithmic sensitivity evaluation has been applied commonly in the assessment of aerosol-cloud interactions (Feingold, 2003; McFiggans et al., 2006; Kay and Wood, 2008; Reutter et al., 2009; Sorooshian et al., 2009; Karydis et al., 2012).

Figure 7a shows the dependence of cloud water droplets (N_{CD}) on N_{CN} and FF. The shape of the isolines is generally consistent with the regime designations reported by Reutter et al. (2009). Following Reutter et al. (2009), a value of the $RS(N_{CN})$ to $RS(FF)$ ratio of 4 or 1/4 was taken as the threshold value to distinguish different regimes (the same criteria were employed for rainwater and frozen water content). Red dashed lines in Fig. 7a indicate the borders between different regimes. This resulted in an aerosol-limited regime in the upper left sector of the panel (N_{CD} is sensitive mainly to N_{CN} and is insensitive to fire forcing), an updraft-limited regime in the lower right sector of the panel (N_{CD} displays a linear dependence on FF and a very weak dependence on N_{CN}), and the transitional regime along the ridge of the isopleth (FF and N_{CN} play comparable roles in the change of N_{CD}). The regimes of Reutter et al. (2009) are derived from simulations of the cloud parcel model of CCN activation at the cloud base. Our results demonstrate that the general regimes for CCN activation still prevail, even when considering full microphysics and the larger temporal and spatial scales of a single pyro-convective cloud system. Figures 7c and 7d display the sensitivity of N_{CD} to variations in N_{CN} and FF. Note that the low/high aerosol and fire forcing conditions (LA, HA, LU, and HU) in these figures refer to a group of N_{CN}/FF conditions. LU: low updrafts (1,000–7,000 W m^{-2}); HU: high updrafts (75,000–300,000 W m^{-2}); LA: low aerosols (200–1,500 cm^{-3}); HA: high aerosols (10,000–100,000 cm^{-3}). High sensitivities were found for low conditions of N_{CN} and FF. While there are some deviations (which appear to be random numerical noise), in general, as either N_{CN} or FF increases, the impact on the cloud droplet number concentration of further changes to either the variable becomes weaker (Figs. 7c and 7d). The reduced sensitivity of cloud droplets to aerosols can be explained by the buffering effect of the cloud microphysics, so that the response of the cloud system to aerosols is much smaller than would have been expected.

Compared with N_{CD}, the cloud mass concentration (M_{CD}) is less sensitive to N_{CN}, and an aerosol-limited regime cannot be said to exist for M_{CD} (Fig. 7b and 7e). As a result, there are only two regimes indicated by the red dashed line in the contour plot (Fig. 7b):

an updraft-limited regime in the lower right sector of the panel, and a transitional regime in the upper sector (an aerosol- and updraft-sensitive regime). The $RS(N_{CN})$ of N_{CD} is on average 10 times higher than that of M_{CD}, independent of the intensity of the FF. As N_{CN} increases, M_{CD} becomes insensitive to the change of N_{CN}. Averaged $RS(FF)$ values over simulated FF ranges for N_{CD} (0.60) and M_{CD} (0.50) are commensurate (Fig. 7d and 7f, respectively), which implies that both the number and mass concentrations of cloud droplets are very sensitive to updrafts. These results are derived from simulations with persistent fire forcing over the modeling period. We have also examined the case in which the fire forcing was shut down after the first half hour of simulation (not shown). The same regimes were found in these simulations, with boundaries in good agreement with the findings presented in this work.

3.2.2 Raindrops

Figure 8 exhibits the temporal evolution of the horizontally-integrated mass concentration of raindrops under four different conditions. Compared with cloud droplets (Fig. 6), the occurrence of raindrops is much later, especially when N_{CN} and fire forcing are in a high level. Only for LULA case, numerous raindrops can be found in a high altitude (5-7 km), while for other cases, most of raindrops are located below 5 km (~0 ℃).

The response of the raindrop number concentration (N_{RD}) to fire forcing and N_{CN} is more complex (Fig. 9a). The impact of FF on N_{RD} is non-monotonic. In general, enhanced FF leads to an increase in N_{RD} under weak updraft condition (<~4,000 W m^{-2}), while further increases in FF result in the reduction in N_{RD}. The aerosol influence varies in the course of N_{CN} change. Under low aerosol condition (<~1,500 cm^{-3}), increased N_{CN} can enhance the production of N_{RD}. Under high aerosol condition (>~2,000 cm^{-3}), the influence of N_{CN} on N_{RD} is very small.

As FF increases in magnitude, the amount of rain produced (M_{RD}) increases (Fig. 9b), but the size of raindrops varies because of the complex behavior of the response of the rain drop number (N_{RD}) to FF (Fig. 9a). The aerosol effect is non-monotonic: M_{RD} increases with aerosols in the lower range of N_{CN} values (<~1000 cm^{-3}), but further increases in N_{CN} result in a decrease in M_{RD}. Combining with the relative sensitivities (Figs. 9e, and 9f), the influence of *FF* is much more significant than that of N_{CN} in most cases. For example, the upper left corner (an aerosol-limited regime for N_{CD}) becomes a transitional regime for M_{RD} with *RS* (*FF*) of 0.1 and *RS* (N_{CN}) of -0.06 (Fig. 9). High sensitivities of M_{RD} to N_{CN} are found at low N_{CN} conditions, but the sensitivity decreases as N_{CN} increases (Fig. 9e). The N_{CN} plays the most negative role in M_{RD} under intermediate N_{CN} conditions (N_{CN} of several 1000 cm^{-3}). In contrast to cloud droplet number concentration, an aerosol-limited regime for M_{RD} hardly exists in our simulations (Fig. 9b). The response of the raindrops to aerosols is much weaker than the response of cloud droplets to aerosols. This finding is consistent with the idea of clouds acting as a buffered system formulated by Stevens and Feingold (2009). Detailed analysis of the microphysical buffering processes will be presented in Sect. 3.3.2.

3.2.3 Frozen water contents

Within our microphysical scheme, frozen water contents are grouped into four main classes: ice crystals, snow, graupel, and hail (Seifert and Beheng, 2006). The time evolution of frozen water content in Fig. 10 suggests that the formation of frozen water content usually occurs in a high level (5-9 km for LU case, and 7-13 km for HU case), and the height of base layer and top layer decreases as time goes by. Under LU condition, the appearance of frozen water content is around 35 min, and lasts for ~120 min, with the peak concentration around 50~70 min. Under HU condition, the frozen particles form around 10 min, and keep in a steady state.

Aerosols exert influence on the frozen water contents via the process of ice nucleation (*in*), but the processes that convert between the different hydrometeor classes and water vapor play a greater role in changing the concentrations of frozen particles, especially the processes of drop freezing to form ice (*cfi*) and the vapor condensational growth of ice and snow (*vdi* and *vds* respectively). Figure 11 illustrates the percentage mass contributions of the individual frozen hydrometeor classes to the total frozen mass.

The percentages of each hydrometeor are calculated based on average values over the entire simulation period. Generally, greater concentrations of aerosols result in more snow and less graupel. This is in agreement with previous studies on convective clouds (Seifert et al., 2012; Lee and Feingold, 2013), and can be explained by the suppression of the warm rain processes under high aerosol condition. High N_{CN} delays the conversion of the cloud water to form raindrops, so that more cloud water content can ascend to altitudes with sub-zero temperatures, hence freeze into small frozen particles (Rosenfeld et al., 2008). Other research has suggested that elevated aerosols could increase the concentration of large frozen particles (graupel/hail) in the convective system (Khain et al., 2009; Wang et al., 2011), which was attributed to the competing effects of aerosols on graupel formation. Since graupel is mainly formed by the accretion of supercooled droplets by ice or snow, the smaller but more abundant supercooled drops under polluted conditions could be either favorable or unfavorable for graupel formation. The percentage of ice crystals does not change much, with ice crystals contributing approximately 20% on average to total frozen particle mass (Fig. 11). It is worth noting that stronger *FF* leads to increasing concentration of hail. But compared to other hydrometeors, its contribution is not important and the relative percentage is very low.

The dependence of total frozen particles on *FF* and N_{CN} is summarized in Fig. 12. With the enhancement in *FF* and N_{CN}, both the number and mass concentrations of the frozen water particles (N_{FP} and M_{FP}, respectively) increase. High $RS(N_{\mathrm{CN}})$ and $RS(FF)$ values were found under low N_{CN} and *FF* conditions (Fig. 12), respectively. As N_{CN} or *FF* increases, their impact becomes weaker, as indicated by a decreasing *RS*. According to the ratio of $RS(FF)/RS(N_{\mathrm{CN}})$, both N_{FP} and M_{FP} are within the updraft-limited regime. Again, smaller $RS(N_{\mathrm{CN}})$ values for M_{FP}, compared with N_{CD}, illustrate the weaker impact of N_{CN} on the production of frozen particles.

3.2.4 Precipitation rate

Surface precipitation rate is a key factor in climate and hydrological processes. Many field measurements, remote sensing studies, and modeling simulations have attempted to evaluate the magnitude of aerosol-induced effects on the surface rainfall rate (Rosenfeld, 1999, 2000; Tao et al., 2007; Li et al., 2008; Sorooshian et al., 2009; Tao et al., 2012). Fig. 13a shows the response of surface precipitation rate (averaged over each 3 h simulation) to *FF* and N_{CN}. The response of surface precipitation to these forcings is similar to that of raindrops (Fig. 9b). The *FF* play a positive role in the precipitation, and *RS*(*FF*) shows a decreasing trend as *FF* increases (Fig. 13c).

The effect of N_{CN} is more complex. Both positive and negative *RS* (N_{CN}) were found in our study. There are generally two different regimes: a precipitation-invigorated regime and a precipitation-inhibited regime. In the precipitation-invigorated regime (N_{CN} < ~1000 cm^{-3}), an increase in N_{CN} leads to an increase in the precipitation rate, and a reduction in *RS* (N_{CN}) (Fig. 13b). In the precipitation-inhibited regime (N_{CN} > ~1000 cm^{-3}), aerosols start to reduce the precipitation, which is reflected in a negative *RS*(N_{CN}). Within the precipitation-inhibited regime, there is also an extreme *RS*(N_{CN}) at a value of N_{CN} of a few thousand particles per cm^{3} (Fig. 13b). The threshold to distinguish these two regimes is derived from the current simulated pyro-convective clouds. The cumulus cloud investigation in Li et al. (2008) also suggested this non-monotonic trend, with the threshold aerosol value around 3000 cm^{-3}. The existence of threshold N_{CN} in both studies implies that similar cloud types may have a similar regime dependence, of which the exact shape may differ due to difference in the meteorological conditions, aerosol properties, etc.

Based on the ensemble studies, we found that individual case studies result in large uncertainties in evaluating the response of precipitation to perturbations, e.g., N_{CN}. Different selections of the parameter space may result in different or even opposite conclusions. Therefore, our ensemble study over a wide range of parameter space sheds some lights on these debates.

Within our simulations, melting of frozen particles is the biggest contributor to precipitation, and the rain rate is well correlated with the melting rate (Fig. 14). For N_{CN} > 1,000 cm^{-3}, increasing N_{CN} results in more small frozen particles (i.e., snow) with low fall velocities. These small frozen particles cannot fall into the warm areas and melt efficiently, resulting in a reduced melting rate. For N_{CN}< 1,000 cm^{-3}, the ratio between large and small frozen particles is not sensitive to N_{CN} anymore and the vertical distribution of frozen particles becomes important. Increasing N_{CN} leads to earlier formation of frozen particles at low altitude, which evaporate less and result in more rainfall.

In the literature, both positive (Tao et al., 2007) and negative (Altaratz et al., 2008) relationship between aerosols and rain rate have been reported in previous case studies. Our simulations suggest that this apparently contradictory phenomenon might be the expression of the same physical processes under different aerosol and dynamic conditions.

Regarding the temporal evolution, low N_{CN} results in earlier rainfall (Fig. 15), which is consistent with current understanding, observations (e.g., Rosenfeld, 1999, 2000), and modeling evidence (e.g., the convective cumulus cloud study by Li et al. (2008)). Note that the general relationship between precipitation and aerosols described in this study is based on simulations over a period of 3 hours. Simulations for a longer period should be carried out in future studies to investigate the influence of aerosols on precipitation over longer time scales as in Fan et al. (2013) and Wang et al. (2014).

3.3 Process Analysis

In our simulations, the evolution of hydrometeor concentrations is determined by multiple microphysical processes. It is often difficult to tell exactly how aerosol particles affect clouds and precipitation. Here we introduce a process analysis method to help understand the aerosol effects.

3.3.1 Clouds

Figure 16 summarizes the contribution of the microphysical processes that act as the main sources (warm color) and sinks (cold color) for cloud droplets under different aerosol and fire forcing conditions. For N_{CD}, the dominant source term is the cloud nucleation (CCN activation) process, in which aerosols are activated under supersaturated water vapor and form cloud droplets. As cloud nucleation happens mostly at the cloud base and so is not strongly affected by cloud dynamical feedbacks, the response of N_{CD} shows similar regimes to cloud parcel models (Reutter et al., 2009). To help explain the regime designation, we divide N_{CD} into two factors: an ambient aerosol number concentration (N_{CN}) and an activated fraction (N_{CD}/N_{CN}). Given the aerosol size distributions, the N_{CD}/N_{CN} ratio is determined approximately by the critical activation diameter (D_c) above which the aerosols can be activated into cloud droplets. The D_c is a function of ambient supersaturation. Stronger updrafts result in higher supersaturation, smaller D_c and hence, larger N_{CD}/N_{CN} ratios. Under high updraft conditions (>15 m s^{-1}), N_{CD}/N_{CN} is already close to unity (Reutter et al., 2009). A further increase in the updraft velocity will still change the supersaturation and D_c, but it will not significantly influence the N_{CD}/N_{CN} ratios and N_{CD}. In this case, N_{CD} is approximately proportional to N_{CN}.

Under weak updrafts, the N_{CD}/N_{CN} ratio is sensitive to ambient supersaturations. In this case, a larger supersaturation induced by stronger updrafts can effectively change the N_{CD}/N_{CN} ratio and thus N_{CD} is sensitive to the updraft velocity. On the other hand, the stronger dependence of N_{CD}/N_{CN} on the supersaturation also changes the role of aerosols. As more aerosols reduce supersaturation, increasing N_{CN} tends to reduce the activated fraction, N_{CD}/N_{CN}. Taking N_{CN} = 60,000 cm^{-3} (FF = 2,000 W m^{-2}), for example, a 10% increase in N_{CN} causes a 4% decrease in N_{CD}/N_{CN}, whereas a 10% decrease in N_{CN} leads to an 8% increase in N_{CD}/N_{CN}. The impact of changing N_{CN} on the N_{CD}/N_{CN} ratio counteracts partly or mostly the positive effect of N_{CN} on cloud droplet formation.

The changes of M_{CD} are influenced mainly by the following sources: (1) the condensation of water vapor on the present cloud droplets (*vdc*) and (2) the cloud nucleation process (*cn*), and by the following sinks: (3) cloud droplet evaporation (*cep*) and (4) the accretion of cloud droplets (*ac*), and (5) the freezing of cloud droplets to form cloud ice (*cfi*), which includes heterogeneous (Seifert and Beheng, 2006) and homogeneous freezing processes (Jeffery and Austin, 1997; Cotton and Field, 2002). Concerning their relative contributions, the net change of condensational growth of droplets (*vdc*) and cloud droplet evaporation (*cep*) dominates the change of M_{CD}. As N_{CN} increases, the condensation rate (*vdc*) does not change much, while the evaporation rate (*cep*) is raised greatly owing to increased surface-to-volume ratio of smaller cloud droplets. Condensation increases M_{CD} and evaporation reduces M_{CD}. In our study, the net effects are negative. A similar result has been reported by Khain et al. (2005) for deep convective clouds. They found that high CCN concentrations led to both greater heating and cooling, and that the net convective heating became smaller as CCN increased. However, the cloud nucleation rate is enhanced and the loss of cloud water due to other sinks (*ac* for weak *FF* condition, and *cfi* for strong *FF* condition) decreases at the same time. This leads to an increasing trend in the total cloud water content with the increase in N_{CN}.

Concerning the absolute contribution, increasing *FF* enhances the change rate of the conversion of water vapor to the condensed phase (R_{vdc} and R_{cn}), whose effect is straightforward. The processes of autoconversion (*au*) and accretion (*ac*) are the major sinks at weak updrafts. As *FF* increases, the conversion of cloud droplets to frozen particles, especially to ice (the *cfi* process), becomes increasingly important.

The contribution of the microphysical processes in each modeling grid could be observed from the pie charts in Fig. 17 (taking HUHA (w = 27 m s^{-1}; N_{CN}=100,000 cm^{-3}) for example, which is representative of the pyro-convective clouds). Each plot shows the vertical cross sections of the averaged change rate of main processes contributing to cloud water content over 30 simulation minutes. Colors within each pie chart reflect the percentage of contributions in each grid. CCN activation usually starts at cloud base, followed by *vdc* in the center of the cloud. Towards both sides, cloud droplets convert to water vapor via evaporation. It is worth noting that the pie charts only represent the relative importance of each process at individual simulation grid, not the absolute amount. Though there are fewer *vdc*-dominated grids than *cep*-dominated grids, the total cloud formation rate from *vdc* is still similar to or higher than the *cep* processes. At cloud top with sub-freezing temperature, cloud droplets are frozen to ice crystals via homogeneous and heterogeneous nucleation. At the beginning stage of the cloud (30 min), the cloud droplets concentrate at the center of the modeling domain. As the cloud evolves, it starts to expand, and at the same time the margin area dissipates due to the sink processes (i.e., *cep*, *cfi*, and *ac*).

We are aware that the exact process rates may vary depending on the microphysical schemes used in the simulation (Muhlbauer et al., 2010). Therefore, we stress that the process analysis here is based on the Seifert microphysical scheme (Seifert and Beheng, 2006). In the future, further observations from laboratory and field measurements are needed to improve the understanding of aerosol-cloud interactions and to better constrain microphysical parametrizations.

3.3.2 Rain

Dynamic conditions strongly influence the pathways of rain formation and dissipation. For weak updraft cases, the warm rain processes, i.e., autoconversion (*au*) and accretion (*ac*) play a big role. Together with melting of snow (*smr*) or graupel (*gmr*), they are the main sources for raindrops (Fig. 18). Under this condition, raindrops may appear at altitudes as high as 5–7 km (e.g., Fig. 8a). For high updraft cases, strong updrafts deliver cloud droplets to higher freezing altitudes (Fig. 6). The cloud droplets then turn directly into frozen particles (cloud→ice crystals), without formation of raindrops as an intermediate stage (cloud→rain→larger frozen particles). Most raindrops are formed from melted frozen droplets and consequently, they appear below ~4 km (Figs. 8c, d). The weaker cloud→rain conversion with higher updrafts also influences the conversion of rain to frozen particles, and is the reason why the *rrg* process (riming of raindrops to form graupel) becomes relatively less important as *FF* increases under low aerosol condition.

The aerosols also modify the pathways of rain formation. Taking weak updraft cases for example, the accretion process (*ac*) dominates the cloud→rain conversion under low aerosol concentrations, but is replaced by autoconversion (*au*) under high aerosol concentrations (Fig. 18b). The reason for this is that *au* is the process that initializes rain formation. Once rain embryos are produced, accretion of cloud droplets by raindrops is triggered and becomes the dominant process of rainwater production, as observed for shallow clouds (Stevens and Seifert, 2008) and stratiform clouds (Wood, 2005). High aerosol loading delays the occurrence of *au*, inhibiting the initialization of rain and the following accretion processes at the early stage (0–100 min). Melted frozen particles are also a major source of raindrops. Under low N_{CN} conditions, most of them form from melted graupel particles, whereas under high N_{CN} condition, melting of snowflakes becomes more important. This is consistent with the aerosol impact on the relative abundance of frozen particles shown in Fig. 11. A higher aerosol concentration leads to a higher fraction of smaller frozen particles (ice crystals and snowflakes). The main difference between low and high updrafts is that cloud conversion is the main source in the former case, whereas in the latter case, melted graupel/snow particles become the main contributors.

Figure 19 illustrates the temporal evolution of the contribution of each process at individual simulation grid (HUHA case). As mentioned before, the warm rain process is quite unimportant under strong *FF* condition (Fig. 18b). However, it is observed that the warm rain process is the leading source of raindrops at the beginning stage (60 min). The raindrops formed from *au* and *ac* are relatively small, which can easily evaporate. The melting of frozen particles to form raindrops becomes more significant after ~90 min, which dominates the production of raindrops. As shown in Fig. 19, although the processes still continue at 180 simulation minutes, the microphysics has already fully developed during this simulation period. Thus our 3 simulation hours could cover the characteristics of the formation and evolution of the pyro-convective clouds. What is more, it should be paid attention that long-term simulation may conceal some detailed information, leading to the bias in prediction of hydrometeors.

The PA clearly demonstrates that aerosols could significantly alter the microphysical pathways and their intensities. Although the variation in individual microphysical process is remarkable, the net result of all processes is not obvious and even insusceptible to aerosol perturbations. This is especially obvious when we consider the aerosol effect on rain water: it is observed that as aerosols is enhanced by a factor of 500, the intensities of the source processes only decrease by a factor of 10; however, there is only a two-fold change in the net rain water content. This implies that the cloud microphysics itself is a self-regulatory system, which can produce equilibrium and buffers the effect of aerosol disturbance (negative feedback).

The sensitivity of raindrops to aerosols mainly depends on autoconversion parameterization, and the melting processes, etc. All those parameterizations have very large uncertainties, especially with bulk microphysical parameterizations. For example, most of the autoconversion schemes were developed or evaluated for stratocumulus clouds, which may not be appropriate for convective clouds. Based on the simulations during the convective phase of squall-line development, van Lier-Walqui et al. (2012) presented the uncertainty in the microphysical parameterization by the posterior probability density functions (PDFs) of parameters, observations, and microphysical processes. With the purpose to improve the representation of microphysics, it is of significance to quantify the parameterization uncertainty by using observation data to constrain parameterization.

3.3.3 Frozen water content

In this section, we only focus on the interactions between liquid water phase and solid water phase. As the selfcollection and internal conversion between different frozen hydrometeors could also cause the change in number concentration of total frozen particles, the process analysis for its number concentration is not discussed. As shown in Fig. 20, the effect of *FF* is straightforward, boosting vapor deposition (*vdi*) and cloud droplet freezing on ice (*cfi*). The *vdi* is always the most important pathway for the formation of frozen particles in our simulations, whereas *cfi* shows comparable contribution in the HULA case. Over a wide range of N_{CN} and updraft velocities, our results have extended and generalized the results of Yin et al. (2005), in which *vdi* and *cfi* were suggested as the dominant processes controlling the formation of ice crystals in individual mixed-phase convective clouds. Although snow is the dominant constituent of frozen particle mass (Fig. 11), the condensation of vapor on ice (*vdi*) rather than on snow is the major pathway for frozen particles. The increase of snow mass is mostly caused by collecting of ice (*ics*) and ice self-collection (coagulation of ice particles, *iscs*), which are internal conversions not counted as either a source or a sink of frozen water content. The ice crystals used for conversion to snow derive mostly from the *vdi* process. Increasing *FF* enhances the upward transport of water vapor and liquid water to higher altitudes where frozen particles can be formed effectively through *vdi* and *cfi*. On the other hand, stronger *FF* reduces the residence time of cloud droplets in the warm environment (to form raindrops), which could explain the attenuation of *rrg* (riming of raindrops to form graupel) as fire forcing increases under low aerosol condition.

Positive relationship between aerosols and the frozen water content have been demonstrated in Sect. 3.2.3. As shown in Fig. 20, the increase in frozen water content is achieved through the enhancement of the *vdi* process. The condensational growth rate R_{vdi} is a function of the number concentration (N_{ice}) and size (D_{ice}) of ice, together with the ambient supersaturation over ice (S_{ice}). In our simulations, the averaged S_{ice} and D_{ice} are not sensitive to the aerosol disturbance; it is the N_{ice} that has been increased significantly because of elevated aerosol concentrations. Higher N_{ice} provides a larger surface area for water vapor deposition on the existing ice crystals and increases R_{vdi}. Lee and Penner (2010) have suggested similar mechanisms for cirrus clouds, which was based on the double-moment bulk representation of Saleeby and Cotton (2004).

The process of the formation and dissipation of frozen water content in the modeling area is illustrated in Fig. 21. The ice crystals form firstly at a higher height, followed by the snow production at a lower level. Downdraughts in the margin region are caused mainly by evaporation and melting. Massive melting takes place at the late stage (after 90 min), when large frozen particles (i.e., graupel) form. This is in agreement with the fact that the raindrops appear at a late stage and at a lower altitude under strong *FF* condition (Figs. 8c and d).

As shown aforementioned, drop freezing parameterizations and ice nucleation parameterizations influence frozen water content dramatically, which involve large uncertainties. Ice microphysics is significantly more complicated due to the wide variety of ice particle characteristics. On one hand, the intensities of these processes differ greatly among different microphysical schemes. Eidhammer et al. (2009) have compared three different ice nucleation parameterizations, and found that different assumptions could result in similar qualitative conclusions although with distinct absolute values. The parameterization with observational constraints agrees well with the measurements. On the other hand, van Lier-Walqui et al. (2012) suggested the processes contributing to frozen particles are dependent on both particle size distribution and density parameters. Parameterization improvement based on observations could help to reduce the uncertainties.

3.3.4 Contribution of individual microphysical processes

The ATHAM model consists of tens of microphysical processes. However, based on the calculation of their relative contributions, only a few processes play dominant roles in regulating the number and mass concentrations of cloud hydrometeors, suggesting a possibility for the simplification of microphysical schemes.

For the number concentration of cloud droplets, the cloud nucleation (*cn*) and *cfi* (freezing of cloud droplets to form ice) processes contribute most to its budget, while other processes together account for less than 10%. For the mass concentration, the net change of *vdc* (condensational growth of cloud droplets by deposition) and *cep* (evaporation of cloud droplets) processes determines the variations in the cloud water content. The *cfi* process could contribute ~50% of the sink under LAHU condition. Therefore, when we simulate the mass of cloud droplets, four microphysical processes, i.e., *cn*, *vdc*, *cep*, and *cfi*, account for a large fraction of the budget.

The dominant processes that contribute ~90% to the raindrop number concentration under specific conditions are autoconversion (*au*), selfcollection (*rsc*), evaporation (*rep*), melting of ice, snow, and graupel (*imr*, *smr*, and *gmr*). For the raindrop mass concentration, the contribution of three processes accounts for ~90% under most conditions, which are rain evaporation (*rep*), melting of snow and graupel (*smr*, and *gmr*).

For the frozen water content, under weak fire forcing condition, *vdi* (condensational growth of ice crystals by deposition) and *sep* (snow evaporation) contribute ~90% of the source and sink respectively. Under strong fire forcing condition, *vdi* and *cfi* together contribute 90% of the source, while *sep* and *gmr* together are the most important sink (90%).

These major processes can capture most of the qualitative and quantitative features of pyro-convection processes and this complex model can thus be simplified for many purposes to improve the computational capacity. Comparison between the comprehensive model and simplified framework will be performed and validated in future studies.

3.4 Uncertainties due to nonlinearity

Aerosol-cloud interactions are regarded as nonlinear processes. In this case, the local aerosol effects on a cloud relevant parameter Y, i.e., $d\mathrm{Y}/dN_{\mathrm{CN}}$ can be different from $\Delta\mathrm{Y}/\Delta N_{\mathrm{CN}}$, the dependence derived from two case studies. Fig. 1 has shown such an example: depending on the case selection, a positive (or negative) $d\mathrm{Y}/dN_{\mathrm{CN}}$ can correspond to a $\Delta\mathrm{Y}/\Delta N_{\mathrm{CN}}$ of 0. Then the question arises, how much difference can be expected between $d\mathrm{Y}/dN_{\mathrm{CN}}$ and $\Delta\mathrm{Y}/\Delta N_{\mathrm{CN}}$? In the following, we take the responses of the precipitation to aerosols as an example to address this issue.

Figure 22 shows the statistics of the relative difference between $\Delta\mathrm{Y}/\Delta N_{\mathrm{CN}}$ and $d\mathrm{Y}/dN_{\mathrm{CN}}$ under LU and HU conditions, in which Y represents the precipitation rate. As precipitation is insensitive to aerosols for N_{CN} >10,000 cm^{-3}, only the cases with N_{CN} of 200~10,000 cm^{-3} are chosen in the calculation. The relative difference is defined as:

$$\text{Relative difference} = \frac{\dfrac{\Delta Y}{\Delta N_{CN}} - \dfrac{dY}{dN_{CN}}}{\dfrac{dY}{dN_{CN}}} \qquad (2)$$

and $\dfrac{\Delta Y}{\Delta N_{CN}}$ is calculated as: $\dfrac{\Delta Y}{\Delta N_{CN}} = \dfrac{Y(2N_{CN}) - Y(N_{CN})}{2N_{CN} - N_{CN}}$, in which the aerosol effect is determined by the difference between the reference case and that after doubling N_{CN}. $\dfrac{dY}{dN_{CN}}$ is the derivative of the precipitation rate at each N_{CN}, representing the local dependence of precipitation on N_{CN}.

The histograms in Fig. 22 demonstrate that $\frac{\Delta Y}{\Delta N_{CN}}$ can deviate considerably from $\frac{dY}{dN_{CN}}$, not only for the absolute value but also for the sign. Statistically, most of the relative differences are in the range of -3.7~0.9 (the 25th and 75th percentiles respectively, with the average difference of -3.0) under LU condition, while are between -1.5 and 0.04 (the 25th and 75th percentiles respectively, with the mean value of 0.02) under HU condition. The fact that individual case studies may not reveal local aerosol effects demonstrates the importance of ensemble studies in determining the real responses of clouds to aerosol perturbations.

4. Conclusions

In this study, the regime dependence of aerosol effects on the formation and evolution of pyro-convective clouds have been studied in detail (Fig. 23). The main conclusions are summarized as follows:

(1) As aerosol number concentration (N_{CN}) and fire forcing (FF) increase, the number concentration of cloud droplets increases. There are three distinct regimes for the cloud number concentration: an updraft-limited regime (high relative sensitivity (RS) ratio of $RS(FF)/RS(N_{\mathrm{CN}})$), an aerosol-limited regime (low $RS(FF)/RS(N_{\mathrm{CN}})$ ratio), and a transitional regime (intermediate $RS(FF)/RS(N_{\mathrm{CN}})$ ratio), which agrees well with the regimes derived from a parcel model (Reutter et al., 2009). The cloud mass concentration is less sensitive to aerosols, and there are two regimes for mass concentration: an updraft-limited regime, and a transitional regime.

(2) The production of rain water content (i.e., M_{RD}) was enhanced with increase in updrafts, and the aerosols could either slightly increase M_{RD} with low aerosol concentration or decrease M_{RD} with large aerosol concentration. The aerosol concentration plays a mostly negative role in M_{CD} under intermediate aerosol conditions (aerosol number concentration of several 1000 cm^{-3}). M_{RD} was generally within an updraft-limited regime, i.e.,

M_{RD} was very sensitive to changes in updrafts, but insensitive to aerosol concentrations ($RS(FF)/RS(N_{CN})$>4). The aerosol and updraft effects on raindrop number concentrations (N_{RD}) are quite complicated; both of them play the non-monotonic role in the N_{RD}.

(3) As updrafts and aerosols increase, the domain-averaged number and mass concentrations of frozen particles (N_{FP} and M_{FP} respectively) were enhanced. N_{FP} and M_{FP} were also within the updraft-limited regime, which is characterized by large $RS(FF)/RS(N_{CN})$ ratio. In this regime, N_{FP} and M_{FP} were directly proportional to fire forcing, and independent of aerosols.

(4) Larger fire forcing resulted in more precipitation, whereas the effect of aerosols on precipitation was complex and could either enhance or suppress the production of precipitation. The suppression on the precipitation is due to the change in the fraction of small frozen particles and total melting rate of frozen particles. The enhancement on the precipitation resulting from increasing N_{CN} under low aerosol condition is a result of changes in the vertical distribution of frozen particles and its evaporation process.

(5) In addition, when aerosol number concentration and fire forcing became too large, their impact became weaker, as indicated by a decreasing relative sensitivity (*RS*).

The process analysis (PA) provided further insight into the mechanisms of aerosol-cloud interactions. By evaluating the contribution of the relevant microphysical processes to the formation of an individual hydrometeor, the PA revealed the dominant factors responsible for the changes in hydrometeor number and mass. (1) Cloud nucleation (*cn*) initializes cloud droplet formation and is the major factor that controls the number concentration of cloud droplets. As expected, the increase in cloud droplet mass can be attributed mostly to the condensational growth (*vdc*). (2) Under weak fire forcing condition, autoconversion (*au*) and accretion (*ac*) are the main sources of rain droplets. Under strong fire forcing condition, the major source is the melting of frozen particles. (3) For the frozen content, the condensation of water vapor on existing ice crystals (*vdi*) is the most important contributor. In addition to CCN activation, the PA also highlights the importance of other microphysical processes in regulating cloud evolution, which is worthy of further scrutiny. By identifying the contribution from individual processes, PA may also provide an opportunity for the simplification of microphysical schemes. For example, out of 24 microphysical processes that are directly related to the budget of cloud droplets and raindrops, over 90% of the mass and number changes are attributed to only 10 processes.

While the general trend is clear, the inclusion of nonlinear (dynamic and microphysical) processes leads to a complex and unstable response of clouds to aerosol perturbations. This applies to the response of all hydrometeors and precipitation, as indicated by the large standard deviation of relative sensitivities in Figs. 7, 9, 12 and 13. This should also hold when variations in other parameters (e.g., meteorological conditions) are introduced. Compared with our results, the relative sensitivities derived from cloud parcel modeling are much smoother (Fig. 8 in Reutter et al. (2009)). The difference is probably caused by complex interactions between cloud microphysics and dynamics (Khain et al., 2008; Fan et al., 2009). These highly nonlinear processes result in a more unstable and chaotic response of cloud evolution to aerosol and dynamic perturbations. Because of this non-linearity, sensitivities of clouds based on limited case studies may require caveats, because they may not be as representative as expected, and so cannot safely be extrapolated to conditions outside of the range explored. To understand better the role of aerosols in cloud formation, we recommend high-resolution ensemble sensitivity studies over a wide range of dynamic and aerosol conditions.

General current understanding and global modelling studies suggest that for cloud droplet number concentration, the updraft-limited regime may be more characteristic of continental clouds, while the aerosol-limited regime may be more characteristic of marine clouds (e.g., Karydis et al., 2012), suggesting that aerosol effects are generally more important for the marine environment. For this case study of pyro-convective clouds, then, we conclude that aerosol effects on cloud droplet number concentrations and cloud droplet size are likely more important than effects on precipitation, since precipitation is far less sensitive to aerosol number concentrations than to updraft velocity. This is in agreement with other studies (e.g., Seifert et al., 2012). A recent long-term convective cloud investigation found that microphysical effects driven by aerosol particles dominate the properties and morphology of deep convective clouds, rather than updraft-related dynamics (Fan et al., 2013). Therefore, it must still be determined whether this conclusion applies to other cloud types and over longer time scales.

In this study, we demonstrate the performance of ensemble simulations in determining the regime dependence of aerosol effects. The use of such regime dependence requires caveats because it may differ for different cloud types, aerosol properties, meteorological conditions and model configurations (e.g., microphysical schemes, dynamic schemes, dimensionality, etc.; the 3-D results are in the supplementary material).

In future work, we intend to extend the current studies to: (1) include other types of clouds with other meteorological or atmospheric conditions; (2) investigate the cloud response over longer timescales (Van Den Heever and Cotton, 2007), as different observational scales could introduce biases in the quantification of aerosol effects on clouds (McComiskey and Feingold, 2012); and (3) evaluate the relative contribution of microphysical and dynamic effects to cloud buffering effects (Stevens and Feingold, 2009; Seifert et al., 2012).

Table A1. Symbols and acronyms for individual microphysical process.

Symbol	Process
cn	Cloud nucleation
cri/s/g/h	Riming of cloud droplets to form ice crystals/snow/graupel/hail
cfi[1]	Freezing of cloud water to form ice crystals
imc/r	Melting of ice crystals to form cloud water/raindrops
au	Autoconversion of cloud water to form rain
ac	Accretion of cloud water by rain
vdc/i/g/s	Condensational growth of cloud droplets/ice crystals/graupel/snow by vapor deposition
in	Ice nucleation
s/g/hmr	Melting of snow/graupel/hail to form raindrops
rsc	Self-collection of raindrops
rfi/s/g/h	Freezing of raindrops to form ice crystals/snow/graupel/hail
rri/s/g/h	Riming of raindrops to form ice crystals/snow/graupel/hail
c/r/i/s/gep	Evaporation of cloud droplets/raindrops/ice/snow/graupel

[1] Here, *cfi* process includes both heterogeneous and homogeneous freezing processes.

Acknowledgements

This work was supported by the Max Planck Society (MPG), Max Planck Graduate Center (MPGC), and EU project BACCHUS (No. 603445). Susannah Burrows was supported by the Office of Science Biological and Environmental Research Program of the U.S. Department of Energy as part of the Earth System Modelling Program. We thank A. Seifert, P. Spichtinger and P. Neis for helpful discussions and model setup.

References

Ackerman, A. S., Toon, O. B., Stevens, D. E., Heymsfield, A. J., Ramanathan, V., and Welton, E. J.: Reduction of tropical cloudiness by soot, Science, 288, 1042-1047, doi: 10.1126/science.288.5468.1042, 2000.

Ackerman, A. S., Toon, O. B., Stevens, D. E., and Coakley, J. A.: Enhancement of cloud cover and suppression of nocturnal drizzle in stratocumulus polluted by haze, Geophys Res Lett, 30, 1381, doi: 10.1029/2002gl016634, 2003.

Albrecht, B. A.: Aerosols, Cloud Microphysics, and Fractional Cloudiness, Science, 245, 1227-1230, doi: 10.1126/science.245.4923.1227, 1989.

Altaratz, O., Koren, I., Reisin, T., Kostinski, A., Feingold, G., Levin, Z., and Yin, Y.: Aerosols' influence on the interplay between condensation, evaporation and rain in warm cumulus cloud, Atmospheric Chemistry and Physics, 8, 15-24, 2008.

Andreae, M. O., Rosenfeld, D., Artaxo, P., Costa, A. A., Frank, G. P., Longo, K. M., and Silva-Dias, M. A. F.: Smoking Rain Clouds over the Amazon, Science, 303, 1337-1342, 2004.

ASRD: Final documentation report-Chisholm Fire (LWF-063), Forest Protection Division, Alberta Sustainable Resource Development, 2001.

Blahak, U.: Towards a Better Representation of High Density Ice Particles in a State-of-the-Art Two-Moment Bulk Microphysical Scheme, 15th International Conf. on Clouds and Precipitation, Cancun, Mexico, July 7–11, 2008.

Bytnerowicz, A., Arbaugh, M., Andersen, C., and Riebau, A.: Wildland Fires and Air Pollution, Dev Environm Sci, 8, 1-638, 2009.

Camponogara, G., Dias, M. A. F. S., and Carrio, G. G.: Relationship between Amazon biomass burning aerosols and rainfall over the La Plata Basin, Atmospheric Chemistry and Physics, 14, 4397-4407, doi: 10.5194/acp-14-4397-2014, 2014.

Cotton, R. J., and Field, P. R.: Ice nucleation characteristics of an isolated wave cloud, Q J Roy Meteor Soc, 128, 2417-2437, doi: 10.1256/Qj.01.150, 2002.

Eidhammer, T., DeMott, P. J., and Kreidenweis, S. M.: A comparison of heterogeneous ice nucleation parameterizations using a parcel model framework, J Geophys Res-Atmos, 114, doi: 10.1029/2008jd011095, 2009.

Fan, J. W., Yuan, T. L., Comstock, J. M., Ghan, S., Khain, A., Leung, L. R., Li, Z. Q., Martins, V. J., and Ovchinnikov, M.: Dominant role by vertical wind shear in regulating aerosol effects on deep convective clouds, J Geophys Res-Atmos, 114, doi: 10.1029/2009jd012352, 2009.

Fan, J. W., Leung, L. R., Rosenfeld, D., Chen, Q., Li, Z. Q., Zhang, J. Q., and Yan, H. R.: Microphysical effects determine macrophysical response for aerosol impacts on deep convective clouds, P Natl Acad Sci USA, 110, E4581-E4590, doi: 10.1073/pnas.1316830110, 2013.

Feingold, G.: Modeling of the first indirect effect: Analysis of measurement requirements, Geophys Res Lett, 30, doi: 10.1029/2003gl017967, 2003.

Graf, H. F., Herzog, M., Oberhuber, J. M., and Textor, C.: Effect of environmental conditions on volcanic plume rise, J Geophys Res-Atmos, 104, 24309-24320, 1999.

Grandey, B. S., Stier, P., and Wagner, T. M.: Investigating relationships between aerosol optical depth and cloud fraction using satellite, aerosol reanalysis and general circulation model data, Atmospheric Chemistry and Physics, 13, 3177-3184, doi: 10.5194/acp-13-3177-2013, 2013.

Herzog, M.: Simulation der dynamik eines multikomponentensystems am beispiel vulkanischer eruptionswolken, Ph. D, University of Hamburg, Hamburg, Germany, 153 pp., 1998.

Herzog, M., Graf, H. F., Textor, C., and Oberhuber, J. M.: The effect of phase changes of water on the development of volcanic plumes, J Volcanol Geoth Res, 87, 55-74, 1998.

Herzog, M., Oberhuber, J. M., and Graf, H. F.: A prognostic turbulence scheme for the nonhydrostatic plume model ATHAM, J Atmos Sci, 60, 2783-2796, 2003.

Hobbs, P. V., and Locatelli, J. D.: Ice nuclei from a natural forest fire, J Appl Meteorol, 8, 833-834, 1969.

Hobbs, P. V., and Radke, L. F.: Cloud Condensation Nuclei from a Simulated Forest Fire, Science, 163, 279-280, 1969.

IPCC: Climate change 2007: The physical science basis, Contribution of Working Group I to the Fourth Assessment Report of the Intergovernmental Panel on Climate Change, edited by: Solomon, S., Qin, D., Manning, M., Chen, Z., Marquis, M., Averyt, K. B., Tignor, M., and Miller, H. L., Cambridge University Press, Cambridge and New York, 2007.

Jeffery, C. A., and Austin, P. H.: Homogeneous nucleation of supercooled water: Results from a new equation of state, J Geophys Res-Atmos, 102, 25269-25279, doi: 10.1029/97jd02243, 1997.

Karydis, V. A., Capps, S. L., Russell, A. G., and Nenes, A.: Adjoint sensitivity of global cloud droplet number to aerosol and dynamical parameters, Atmospheric Chemistry and Physics, 12, 9041-9055, doi: 10.5194/acp-12-9041-2012, 2012.

Kaufman, Y. J., and Fraser, R. S.: The effect of smoke particles on clouds and climate forcing, Science, 277, 1636-1639, 1997.

Kaufman, Y. J., Tanre, D., and Boucher, O.: A satellite view of aerosols in the climate system, Nature, 419, 215-223, doi: 10.1038/Nature01091, 2002.

Kaufman, Y. J., and Koren, I.: Smoke and pollution aerosol effect on cloud cover, Science, 313, 655-658, doi: 10.1126/science.1126232, 2006.

Kay, J. E., and Wood, R.: Timescale analysis of aerosol sensitivity during homogeneous freezing and implications for upper tropospheric water vapor budgets, Geophys Res Lett, 35, doi: 10.1029/2007gl032628, 2008.

Khain, A., Rosenfeld, D., and Pokrovsky, A.: Aerosol impact on the dynamics and microphysics of deep convective clouds, Q J Roy Meteor Soc, 131, 2639-2663, doi: 10.1256/Qj.04.62, 2005.

Khain, A. P., BenMoshe, N., and Pokrovsky, A.: Factors determining the impact of aerosols on surface precipitation from clouds: An attempt at classification, J Atmos Sci, 65, 1721-1748, doi: 10.1175/2007jas2515.1, 2008.

Khain, A. P.: Notes on state-of-the-art investigations of aerosol effects on precipitation: a critical review, Environ Res Lett, 4, doi: 10.1088/1748-9326/4/1/015004, 2009.

Khain, A. P., Leung, L. R., Lynn, B., and Ghan, S.: Effects of aerosols on the dynamics and microphysics of squall lines simulated by spectral bin and bulk parameterization schemes, J Geophys Res-Atmos, 114, doi: 10.1029/2009jd011902, 2009.

Koren, I., Kaufman, Y. J., Remer, L. A., and Martins, J. V.: Measurement of the effect of Amazon smoke on inhibition of cloud formation, Science, 303, 1342-1345, doi: 10.1126/science.1089424, 2004.

Lee, S. S., Donner, L. J., Phillips, V. T. J., and Ming, Y.: The dependence of aerosol effects on clouds and precipitation on cloud-system organization, shear and stability, J Geophys Res-Atmos, 113, doi: 10.1029/2007jd009224, 2008.

Lee, S. S., and Penner, J. E.: Aerosol effects on ice clouds: can the traditional concept of aerosol indirect effects be applied to aerosol-cloud interactions in cirrus clouds?, Atmospheric Chemistry and Physics, 10, 10345-10358, doi: 10.5194/acp-10-10345-2010, 2010.

Lee, S. S., and Feingold, G.: Aerosol effects on the cloud-field properties of tropical convective clouds, Atmospheric Chemistry and Physics, 13, 6713-6726, doi:10.5194/acp-13-6713-2013, 2013.

Levin, Z., and Cotton, W.: Aerosol Pollution Impact on Precipitation: A Scientific Review, World Meteorol. Organ, Geneva, Switzerland, 2007.

Li, G. H., Wang, Y., and Zhang, R. Y.: Implementation of a two-moment bulk microphysics scheme to the WRF model to investigate aerosol-cloud interaction, J Geophys Res-Atmos, 113, doi: 10.1029/2007jd009361, 2008.

Luderer, G. G.: Modeling of Deep-Convective Vertical Transport of Foreset Fire Smoke into the Upper Troposphere and Lower Stratosphere, Ph.D, Physics Department, Johannes Gutenberg University Mainz, Mainz, 2007.

McComiskey, A., and Feingold, G.: The scale problem in quantifying aerosol indirect effects, Atmospheric Chemistry and Physics, 12, 1031-1049, doi: 10.5194/acp-12-1031-2012, 2012.

McFiggans, G., Artaxo, P., Baltensperger, U., Coe, H., Facchini, M. C., Feingold, G., Fuzzi, S., Gysel, M., Laaksonen, A., Lohmann, U., Mentel, T. F., Murphy, D. M., O'Dowd, C. D., Snider, J. R., and Weingartner, E.: The effect of physical and chemical aerosol properties on warm cloud droplet activation, Atmospheric Chemistry and Physics, 6, 2593-2649, 2006.

Muhlbauer, A., Hashino, T., Xue, L., Teller, A., Lohmann, U., Rasmussen, R. M., Geresdi, I., and Pan, Z.: Intercomparison of aerosol-cloud-precipitation interactions in stratiform orographic mixed-phase clouds, Atmospheric Chemistry and Physics, 10, 8173-8196, doi: 10.5194/acp-10-8173-2010, 2010.

Norris, J. R.: Has northern Indian Ocean cloud cover changed due to increasing anthropogenic aerosol?, Geophys Res Lett, 28, 3271-3274, doi: 10.1029/2001gl013547, 2001.

Oberhuber, J. M., Herzog, M., Graf, H. F., and Schwanke, K.: Volcanic plume simulation on large scales, J Volcanol Geoth Res, 87, 29-53, 1998.

Pruppacher, H. R., and Klett, J. D.: Microphysics of Clouds and Precipitation, Second Revised and Enlarged Edition with an Introduction to Cloud Chemistry and Cloud Electricity, Kluwer Academic Publishers, Reidel, Dordrecht, 954 pp., 1997.

Reid, J. S., Koppmann, R., Eck, T. F., and Eleuterio, D. P.: A review of biomass burning emissions part II: intensive physical properties of biomass burning particles, Atmospheric Chemistry and Physics, 5, 799-825, 2005.

Reutter, P., Su, H., Trentmann, J., Simmel, M., Rose, D., Gunthe, S. S., Wernli, H., Andreae, M. O., and Poschl, U.: Aerosol- and updraft-limited regimes of cloud droplet formation: influence of particle number, size and hygroscopicity on the activation of cloud condensation nuclei (CCN), ATMOSPHERIC CHEMISTRY AND PHYSICS, 9, 7067-7080, 10.5194/acp-9-7067-2009, 2009.

Reutter, P., Trentmann, J., Seifert, A., Neis, P., Su, H., Chang, D., Herzog, M., Wernli, H., Andreae, M. O., and Poschl, U.: 3-D model simulations of dynamical and microphysical interactions in pyro-convective clouds under idealized conditions, Atmospheric Chemistry and Physics, 14, 7573-7583, doi:10.5194/acp-14-7573-2014, 2014.

Rosenfeld, D.: TRMM observed first direct evidence of smoke from forest fires inhibiting rainfall, Geophys Res Lett, 26, 3105-3108, 1999.

Rosenfeld, D.: Suppression of rain and snow by urban and industrial air pollution, Science, 287, 1793-1796, 2000.

Rosenfeld, D., Fromm, M., Trentmann, J., Luderer, G., Andreae, M. O., and Servranckx, R.: The Chisholm firestorm: observed microstructure, precipitation and lightning activity of a pyro-cumulonimbus, Atmos Chem Phys, 7, 645-659, 2007.

Rosenfeld, D., Lohmann, U., Raga, G. B., O'Dowd, C. D., Kulmala, M., Fuzzi, S., Reissell, A., and Andreae, M. O.: Flood or drought: How do aerosols affect precipitation?, Science, 321, 1309-1313, doi: 10.1126/science.1160606, 2008.

Saleeby, S. M., and Cotton, W. R.: A large-droplet mode and prognostic number concentration of cloud droplets in the Colorado State University Regional Atmospheric Modeling System (RAMS). Part I: Module descriptions and supercell test simulations, J Appl Meteorol, 43, 182-195, doi: 10.1175/1520-0450(2004)043, 2004.

Saleeby, S. M., Cotton, W. R., Lowenthal, D., Borys, R. D., and Wetzel, M. A.: Influence of Cloud Condensation Nuclei on Orographic Snowfall, J Appl Meteorol Clim, 48, 903-922, doi: 10.1175/2008jamc1989.1, 2009.

Sassen, K., and Khvorostyanov, V. I.: Cloud effects from boreal forest fire smoke: evidence for ice nucleation from polarization lidar data and cloud model simulations, Environ Res Lett, 3, 12, doi: 10.1088/1748-9326/3/2/025006, 2008.

Seifert, A., and Beheng, K. D.: A two-moment cloud microphysics parameterization for mixed-phase clouds. Part 1: Model description, Meteorol Atmos Phys, 92, 45-66, doi: 10.1007/s00703-005-0112-4, 2006.

Seifert, A., Khain, A., Pokrovsky, A., and Beheng, K. D.: A comparison of spectral bin and two-moment bulk mixed-phase cloud microphysics, Atmos Res, 80, 46-66, doi: 10.1016/j.atmosres.2005.06.009, 2006.

Seifert, A., Kohler, C., and Beheng, K. D.: Aerosol-cloud-precipitation effects over Germany as simulated by a convective-scale numerical weather prediction model, Atmospheric Chemistry and Physics, 12, 709-725, doi: 10.5194/acp-12-709-2012, 2012.

Sorooshian, A., Feingold, G., Lebsock, M. D., Jiang, H. L., and Stephens, G. L.: On the precipitation susceptibility of clouds to aerosol perturbations, Geophys Res Lett, 36, L13803, doi: 10.1029/2009gl038993, 2009.

Stevens, B., and Seifert, A.: Understanding macrophysical outcomes of microphysical choices in simulations of shallow cumulus convection, J Meteorol Soc Jpn, 86, 143-162, 2008.

Stevens, B., and Feingold, G.: Untangling aerosol effects on clouds and precipitation in a buffered system, Nature, 461, 607-613, doi: 10.1038/Nature08281, 2009.

Tao, W. K., Li, X. W., Khain, A., Matsui, T., Lang, S., and Simpson, J.: Role of atmospheric aerosol concentration on deep convective precipitation: Cloud-resolving model simulations, J Geophys Res-Atmos, 112, D24S18, doi: 10.1029/2007jd008728, 2007.

Tao, W. K., Chen, J. P., Li, Z. Q., Wang, C., and Zhang, C. D.: Impact of Aerosols on Convective Clouds and Precipitation, Rev Geophys, 50, doi: 10.1029/2011rg000369, 2012.

Teller, A., and Levin, Z.: Factorial method as a tool for estimating the relative contribution to precipitation of cloud microphysical processes and environmental conditions: Method and application, J Geophys Res-Atmos, 113, doi: 10.1029/2007jd008960, 2008.

Van Den Heever, S. C., and Cotton, W. R.: Urban aerosol impacts on downwind convective storms, J Appl Meteorol Clim, 46, 828-850, doi: 10.1175/Jam2492.1, 2007.

van Lier-Walqui, M., Vukicevic, T., and Posselt, D. J.: Quantification of Cloud Microphysical Parameterization Uncertainty Using Radar Reflectivity, Mon Weather Rev, 140, 3442-3466, doi: 10.1175/Mwr-D-11-00216.1, 2012.

Wang, Y., Wan, Q., Meng, W., Liao, F., Tan, H., and Zhang, R.: Long-term impacts of aerosols on precipitation and lightning over the Pearl River Delta megacity area in China, Atmospheric Chemistry and Physics, 11, 12421-12436, 10.5194/acp-11-12421-2011, 2011.

Wang, Y., Fan, J. W., Zhang, R. Y., Leung, L. R., and Franklin, C.: Improving bulk microphysics parameterizations in simulations of aerosol effects, J Geophys Res-Atmos, 118, 5361-5379, doi: 10.1002/Jgrd.50432, 2013.

Wang, Y., Zhang, R. Y., and Saravanan, R.: Asian pollution climatically modulates mid-latitude cyclones following hierarchical modelling and observational analysis, Nat Commun, 5, doi: 10.1038/Ncomms4098, 2014.

Wood, R.: Drizzle in stratiform boundary layer clouds. Part II: Microphysical aspects, J Atmos Sci, 62, 3034-3050, doi: 10.1175/Jas3530.1, 2005.

Yin, Y., Carslaw, K. S., and Feingold, G.: Vertical transport and processing of aerosols in a mixed-phase convective cloud and the feedback on cloud development, Q J Roy Meteor Soc, 131, 221-245, doi: 10.1256/qj.03.186, 2005.

Zhang, L. M., Michelangeli, D. V., and Taylor, P. A.: Influence of aerosol concentration on precipitation formation in low-level, warm stratiform clouds, J Aerosol Sci, 37, 203-217, doi: 10.1016/j.jaerosci.2005.04.002, 2006.

Table captions

Table 1. Typical characterizations of the frozen hydrometeor classes.

Table 1. Typical characterizations of the frozen hydrometeor classes.

		Diameter (mm)	Density (g cm^{-3})	Terminal velocity (m s^{-1})
Cloud ice	Columnar cystals	0.01—1[(1)]	0.36—0.7 [(2)]	0.013—0.055[(2)]
	Plate-like	0.01—1[(1)]	~0.9[(1)]	0.02—0.06[(2)]
	Dendrites	0.1—3[(1)]	0.3—1.4[(1)]	0.25—0.7[(3)]
Snowflakes		2—5[(1)]	0.05—0.89[(1)]	0.5—3[(1)]
Graupel		0.5—5[(1)]	~0.4[(1)]	3—14[(1)]
Hail		5—80[(1)]	0.8—0.9[(1)]	10—40[(1)]

[(1)] Pruppacher H.R. (1978).

[(2)]Jayaweer and Ryan (1972).

[(3)]Mitchell and Heymsfield (2005).

Figure captions

Figure 1. Conceptual model of the nonlinear relationship between aerosol concentrations and rain rate (Data are from 2-D simulation results of this work).

Figure 2. Atmospheric sounding launched near Edmonton, Alberta on 29 May 2001. The right black line represents the temperature, and the left black line corresponds to the dew-point temperature. This weather information is from the University of Wyoming Department of Atmospheric Science (http://weather.uwyo.edu/).

Figure 3. The 110×100 grid points in the computational domain.

Figure 4. Probability distribution function of vertical velocities (w) at cloud base layer under different fire forcing conditions (a); Relationship between input fire forcing (FF) and induced vertical velocity (w) at cloud base (b). The aerosol concentration is 1,000 cm^{-3}. The shaded area represents the variability of estimation ($\pm\frac{1}{2}\sigma$).

Figure 5. The correlation of fire forcing and the corresponding maximum temperature at cloud base. The shaded area indicates the variability of estimation ($\pm\frac{1}{2}\sigma$) over each simulation period.

Figure 6. Time evolution of horizontally-averaged cloud water content (g kg^{-1}) as a function of altitude for four extreme cases, which are referred to as (1) LULA: low updrafts (2,000 W m^{-2}) and low aerosols (200 cm^{-3}); (2) LUHA: low updrafts (2,000 W m^{-2}) and high aerosols (100,000 cm^{-3}); (3) HULA: high updrafts (300,000 W m^{-2}) and low aerosols (200 cm^{-3}); (4) HUHA: high updrafts (300,000 W m^{-2}) and high aerosols (100,000 cm^{-3}). Maximum values for each episode are also shown.

Figure 7. Number (a) and mass concentration (b) of cloud droplets calculated as a function of aerosol number concentration (N_{CN}) and updraft velocity (represented by FF). Red dashed lines indicate the borders between different regimes defined by $RS(N_{CN})/RS(FF)$=4 or 1/4, respectively. Relative sensitivities with respect to N_{CN} (left) and FF (right) for number (panels (c) and (d)) and mass (panels (e) and (f)) concentration of cloud droplets under different conditions. The thick dashed or solid lines represent the mean values under a given condition, and the shaded areas represent the variability of estimation ($\pm\frac{1}{2}\sigma$). The acronyms indicate LU: low updrafts (1,000–7,000 W m^{-2}); HU: high updrafts (75,000–300,000 W m^{-2}); LA: low aerosols (200–1,500 cm^{-3}); HA: high aerosols (10,000–100,000 cm^{-3}).

Figure 8. Same as Figure 6 but for raindrops.

Figure 9. Same as Figure 7 but for raindrops.

Figure 10. Same as Figure 6 but for the frozen particles.

Figure 11. Contributions of individual frozen hydrometeor to total frozen water content under four extreme conditions which are referred to as (1) LULA: low updrafts (2,000 W m^{-2}) and low aerosols (200 cm^{-3}); (2) LUHA: low updrafts (2,000 W m^{-2}) and high aerosols (100,000 cm^{-3}); (3) HULA: high updrafts (300,000 W m^{-2}) and low aerosols (200 cm^{-3}); (4) HUHA: high updrafts (300,000 W m^{-2}) and high aerosols (100,000 cm^{-3}).

Figure 12. Same as Figure **7** but for total frozen particles.

Figure 13. Same as Figure 7 but for surface rain rate.

Figure 14. The correlation of rain rate and the melting rate of the frozen particles. The green diamond points are the averaged rain rate under different aerosol concentrations ($FF = 10^5$ W m^{-2}). The columns represent the integrated melting rate from individual frozen particles.

Figure 15. Time evolution of surface rain rates for the three aerosol episodes (N_{CN} = 200; 1,000; and 100,000 cm^{-3} respectively) under LU (low updrafts, FF=2,000 W m^{-2}) and HU (high updrafts, FF=50,000 W m^{-2}) conditions.

Figure 16. The pie charts summarize the relative percentage of the microphysical processes involving cloud droplets as a function of N_{CN} and fire forcing (a: number concentration; b: mass concentration). Colors within each pie chart reflect the contribution of processes under the specific condition. Warm colors denote the sources, while cold colors denote the sinks. The acronyms indicate cn: cloud nucleation; vdc: condensational growth of cloud droplets; cep: evaporation of cloud droplets; au: autoconversion; ac: accretion; cfi: freezing of cloud droplets to form ice crystals, including homogeneous and heterogeneous nucleation; crg/h: riming of cloud droplets to form graupel/hail.

Figure 17. The pie charts summarize the vertical cross sections of the change rate of main microphysical processes contributing to cloud water content. Each pie chart shows the averaged contribution over the past 30 min. Colors within each pie chart reflect the percentage of processes in each grid. The black dashed line is the 0.1 μg kg^{-1} isoline of the interstitial aerosol, indicating the shape of smoke plume. The meaning of the acronyms is the same as in Figure 16. Warm colors denote the sources, while cold colors denote the sinks.

Figure 18. Same as Figure 16 but for raindrops. The acronyms indicate au: autoconversion; ac: accretion; i/s/g/hmr: melting of ice/snow/graupel/hail to form raindrops; rsc: self-collection of raindrops; ismr: melting of ice and snow to form raindrops; rfi/h: freezing of raindrops to form ice crystals/hail; rep: raindrop evaporation; rrg: riming of raindrops to form graupel; rris: riming of raindrops to form ice and snow.

Figure 19. Same as Figure 17, but for raindrops.

Figure 20. Same as Figure 16 but for the total frozen water content. The acronyms indicate in: ice nucleation; cfi: freezing of cloud droplets to form ice crystals, including homogeneous and heterogeneous nucleation; rfh: freezing of raindrops to form hail; vdi/s/g: condensational growth of ice crystals/snow/graupel by water vapor; rrg: riming of raindrops to form graupel; i/s/gep: evaporation of ice/snow/graupel; s/g/hmr: melting of snow/graupel/hail to form raindrops.

Figure 21. Same as Figure 17 but for frozen particles.

Figure 22. Histograms of the relative difference between $\frac{\Delta Y}{\Delta N_{CN}}$ and $\frac{dY}{dN_{CN}}$ under LU and HU conditions, where Y here denotes precipitation rate. $\frac{\Delta Y}{\Delta N_{CN}} = \frac{Y(2N_{CN}) - Y(N_{CN})}{2N_{CN} - N_{CN}}$, and $\frac{dY}{dN_{CN}}$ is the derivative of the precipitation rate along the variable N_{CN}.

Figure 23. Overview of the research approaches on multi-scale cloud initialization and development. The aerosol-cloud interaction at the microphysical scale, i.e., cloud condensation nuclei (CCN) activation, has been well characterized by the Köhler theory (Kohler, 1936) and by a series of extended equations (Shulman et al., 1996; Kulmala et al., 1997; Laaksonen et al., 1998). When we upscale the activation of a single aerosol particle to aerosol populations at the cloud base, the impact of aerosols on the number of activated CCN still appears simple and can be well described (i.e., the three generic regimes of CCN activation). When considering full microphysics and the larger temporal and spatial scales of a single pyro-convective cloud, the performance of ensemble simulations shows the regime dependence of aerosol effects on the pyro-convective cloud formation and evolution.

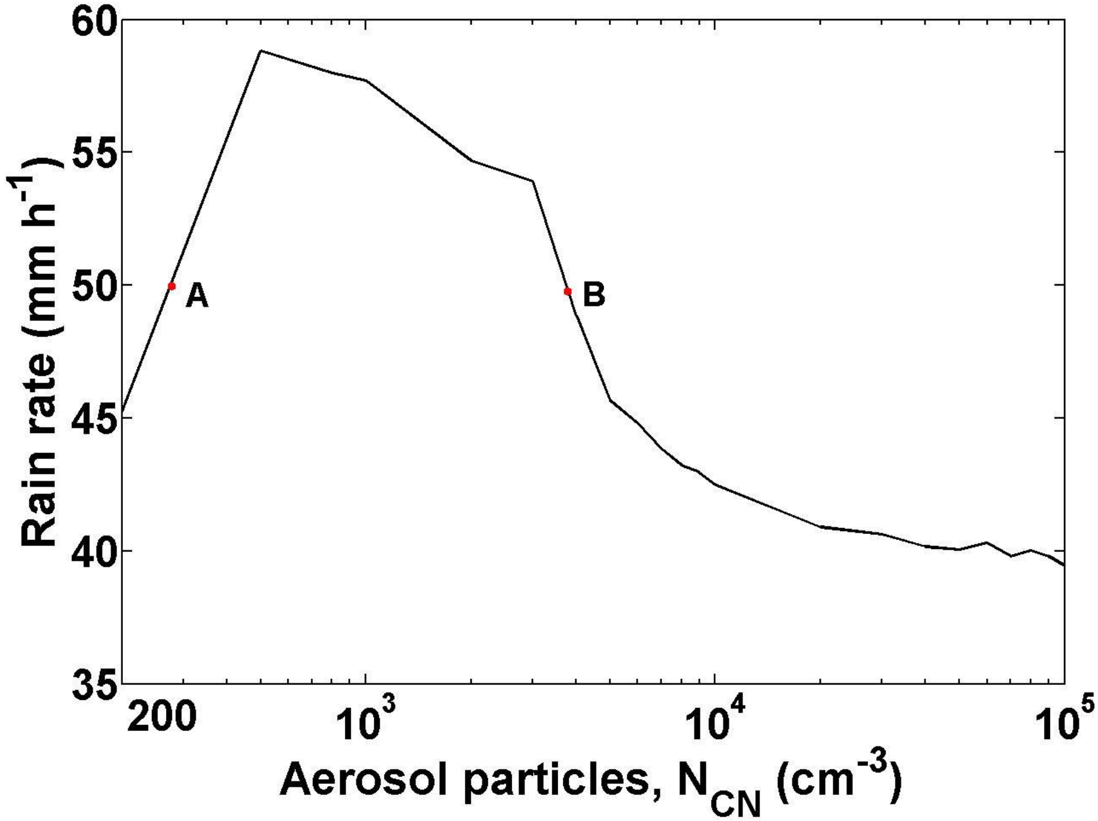

Figure 1. Conceptual model of the nonlinear relationship between aerosol concentrations and rain rate (Data are from 2-D simulation results of this work).

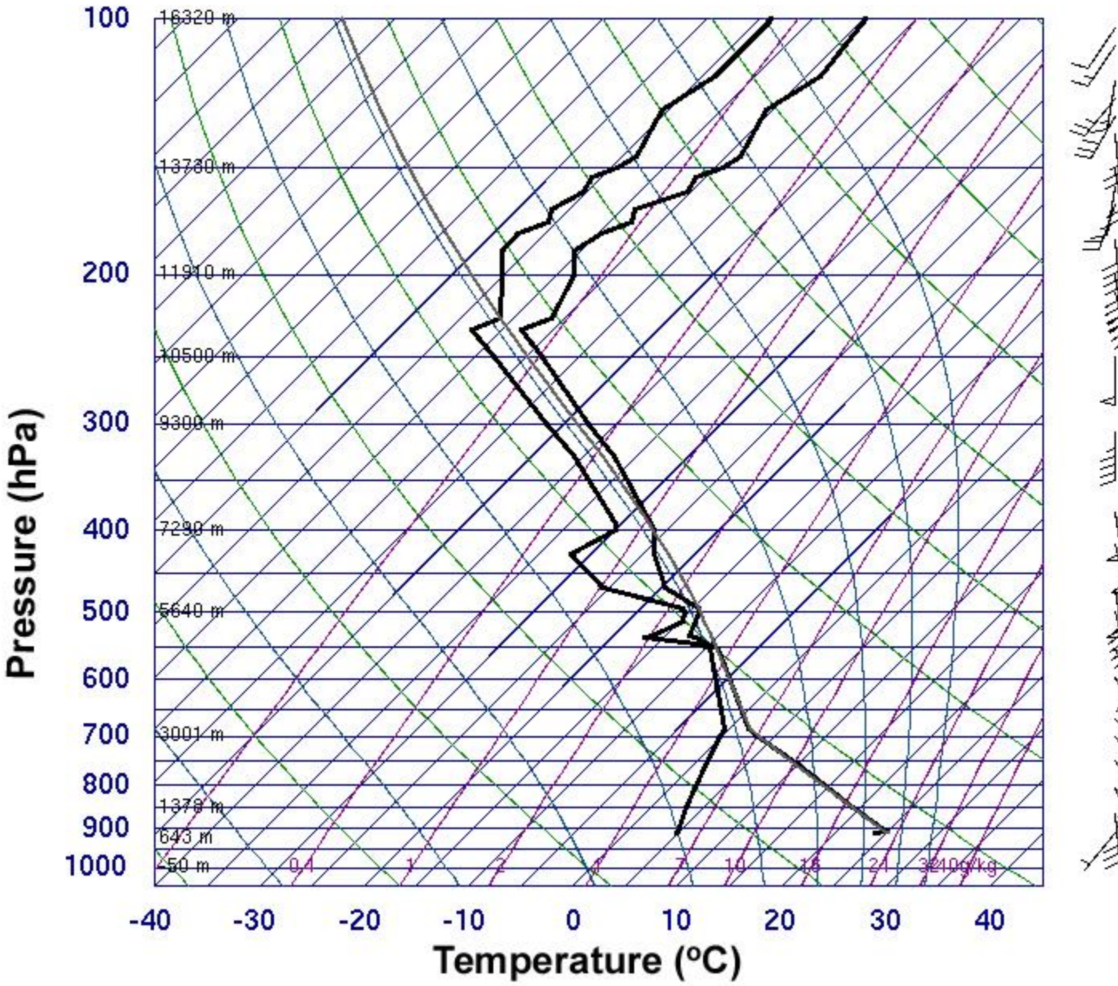

Figure 2. Atmospheric sounding launched near Edmonton, Alberta on 29 May 2001. The right black line represents the temperature, and the left black line corresponds to the dew-point temperature. This weather information is from the University of Wyoming Department of Atmospheric Science (http://weather.uwyo.edu/).

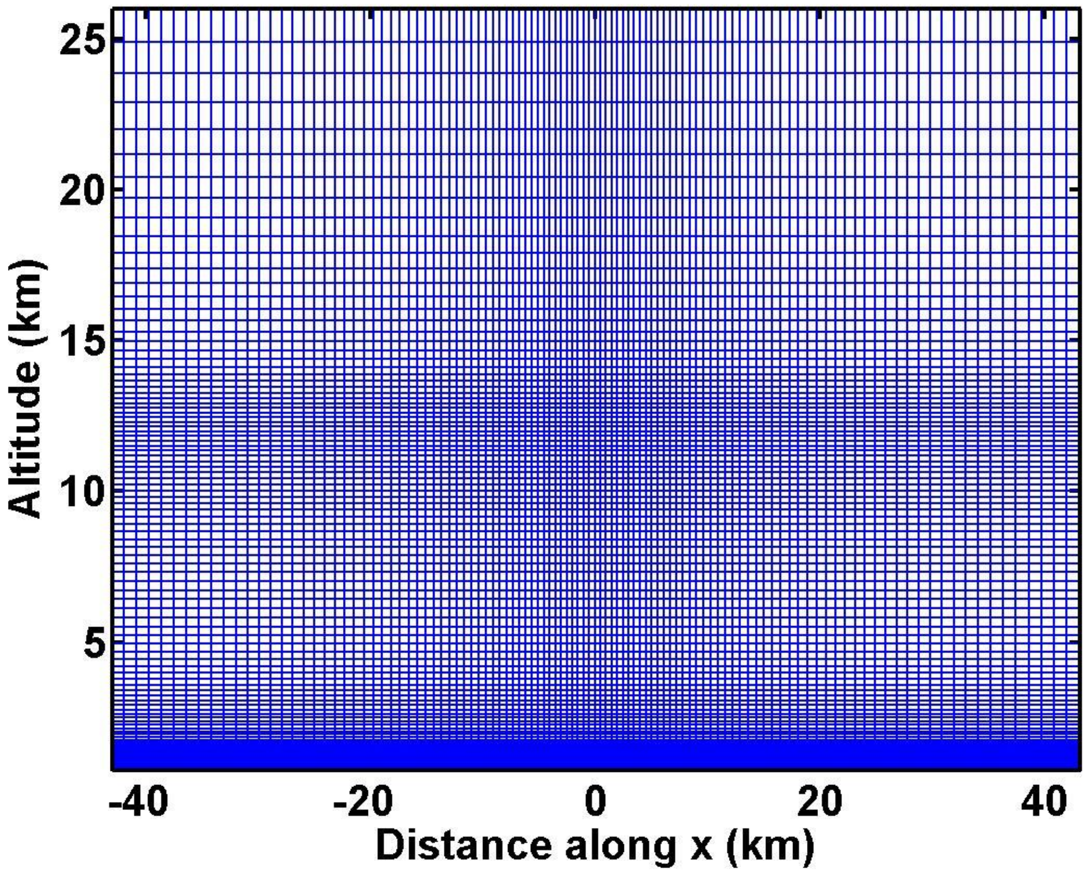

03

Figure 3. The 110×100 grid points in the computational domain.

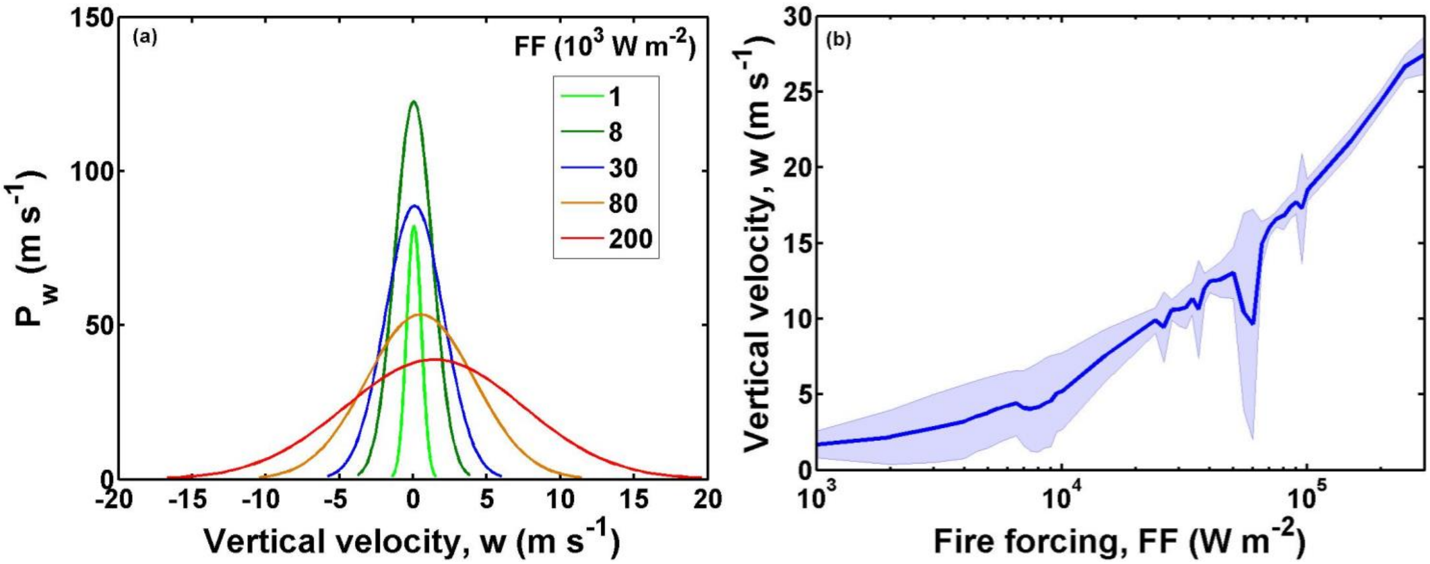

Figure 4. Probability distribution function of vertical velocities (*w*) at cloud base layer under different fire forcing conditions (a); Relationship between input fire forcing (*FF*) and induced vertical velocity (*w*) at cloud base (b). The aerosol concentration is 1,000 cm^{-3}. The shaded area represents the variability of estimation (±½σ).

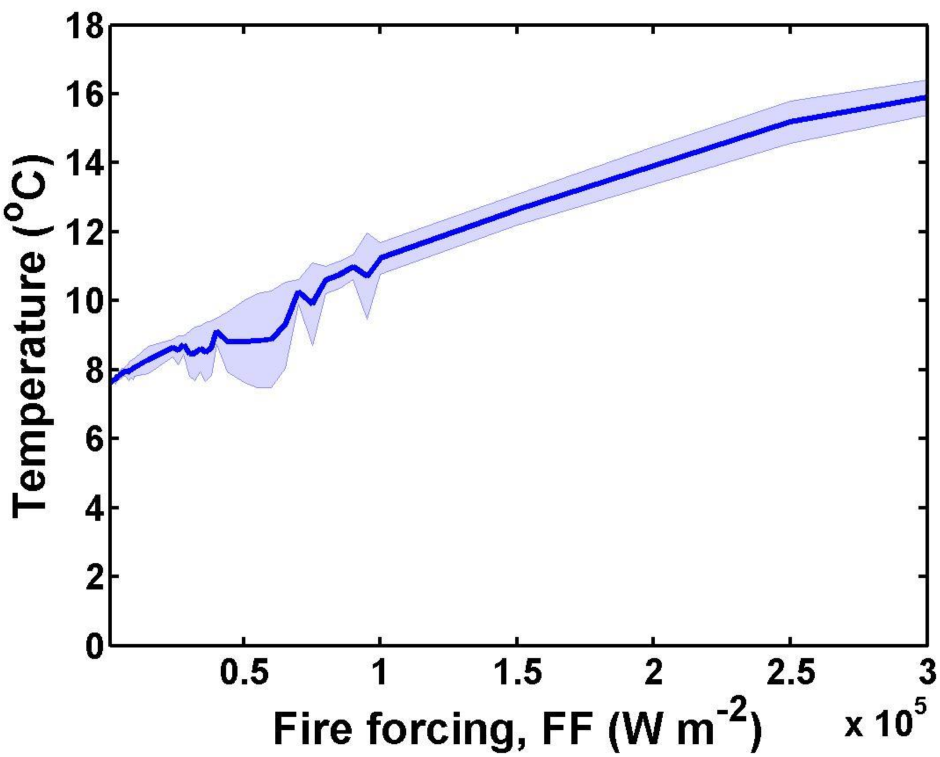

Figure 5. The correlation of fire forcing and the corresponding maximum temperature at cloud base. The shaded area indicates the variability of estimation (±½σ) over each simulation period.

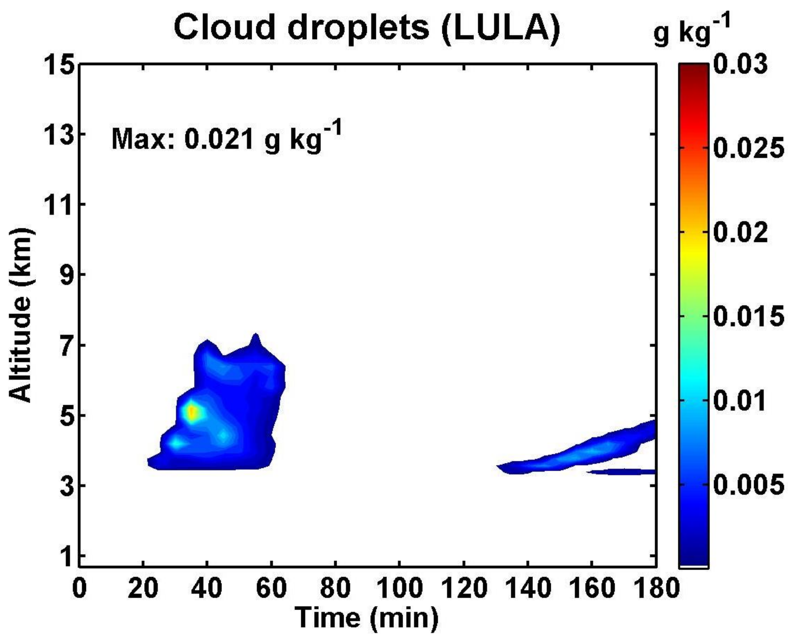

(a)

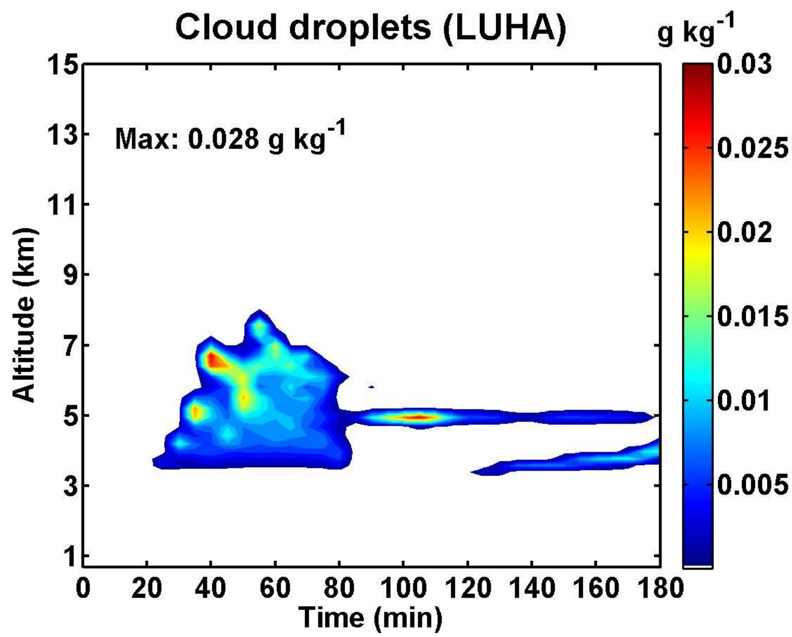

(b)

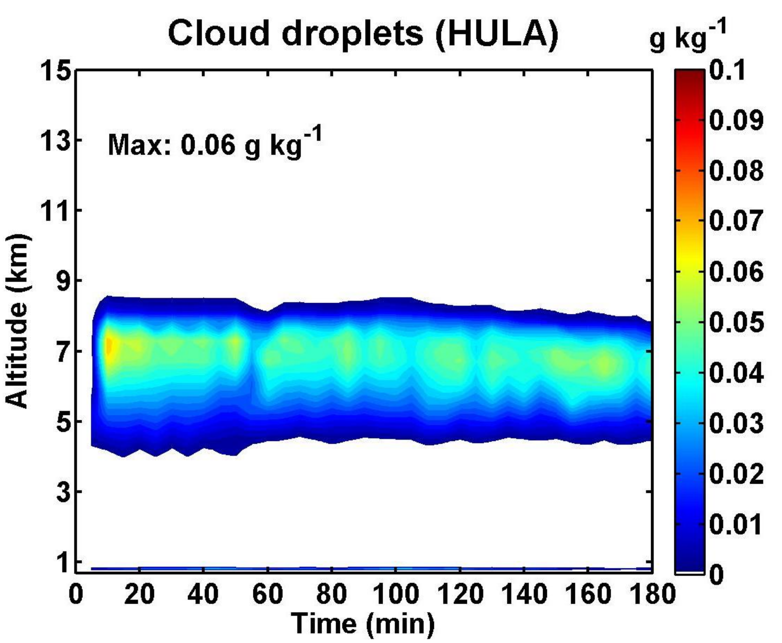

(c)

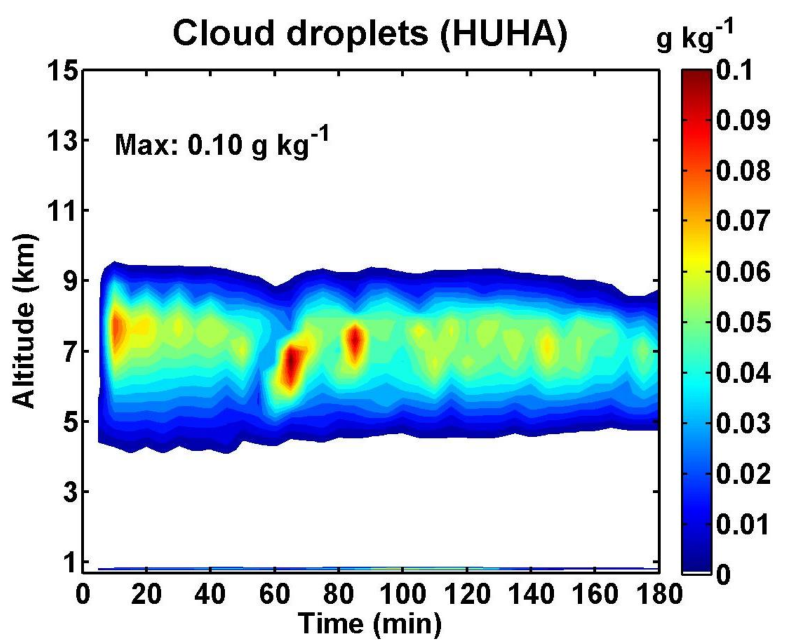

(d)

Figure 6. Time evolution of horizontally-averaged cloud water content (g kg^{-1}) as a function of altitude for four extreme cases, which are referred to as (1) LULA: low updrafts (2,000 W m^{-2}) and low aerosols (200 cm^{-3}); (2) LUHA: low updrafts (2,000 W m^{-2}) and high aerosols (100,000 cm^{-3}); (3) HULA: high updrafts (300,000 W m^{-2}) and low aerosols (200 cm^{-3}); (4) HUHA: high updrafts (300,000 W m^{-2}) and high aerosols (100,000 cm^{-3}). Maximum values for each episode are also shown.

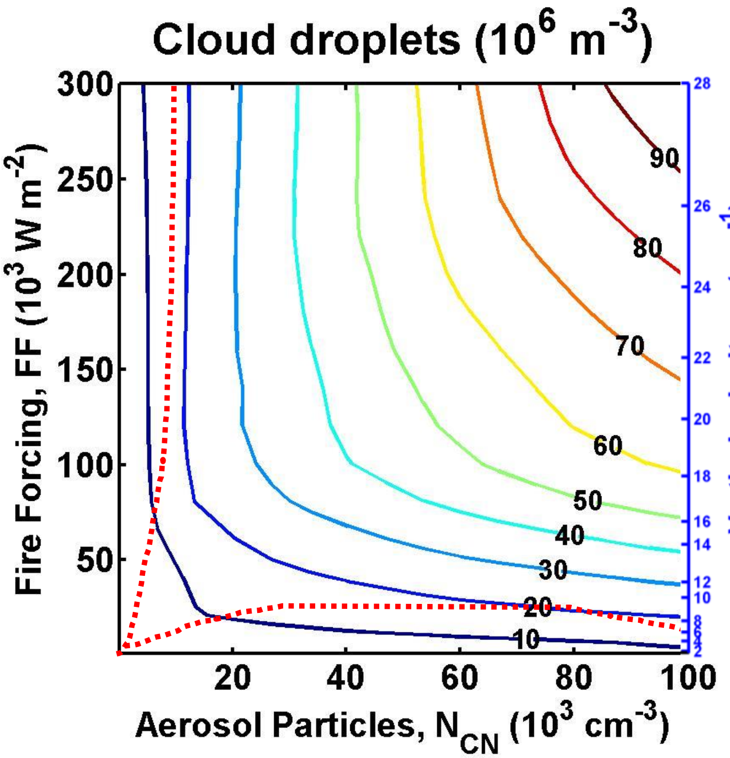

Cloud droplets (10^6 m^{-3})
Fire Forcing, FF (10^3 W m^{-2})
Aerosol Particles, N_{CN} (10^3 cm^{-3})
Vertical velocity, w (m s^{-1})
300
250
200
150
100
50
20
40
60
80
100
90
80
70
60
50
40
30
20
10
28
26
24
22
20
18
16
14
12
10

(a)

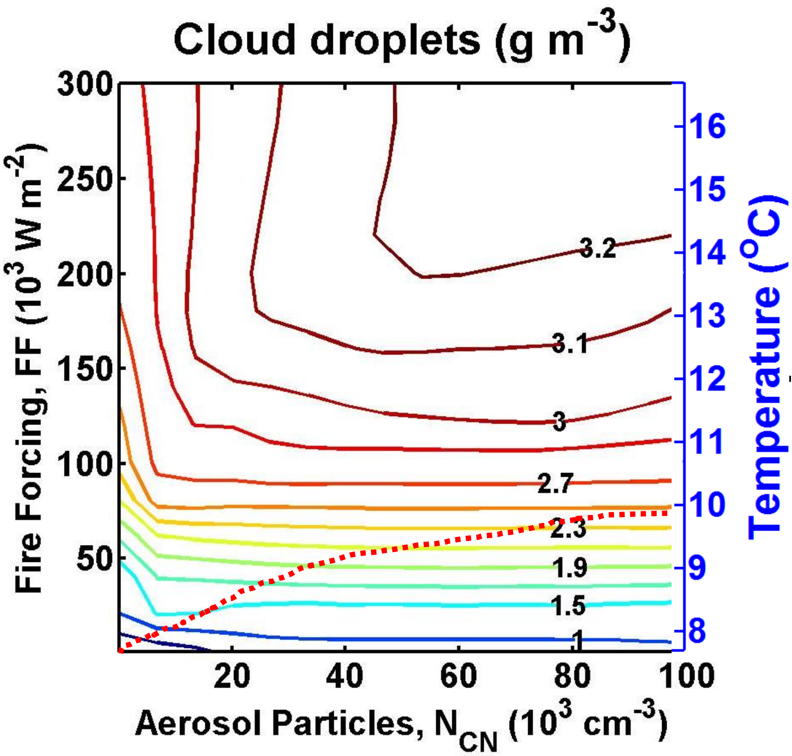

Cloud droplets (g m^{-3})
Fire Forcing, FF (10^3 W m^{-2})
Aerosol Particles, N_{CN} (10^3 cm^{-3})
Temperature (^{o}C)
300
250
200
150
100
50
20
40
60
80
100
16
15
14
13
12
11
10
9
8
3.2
3.1
3
2.7
2.3
1.9
1.5
1

(b)

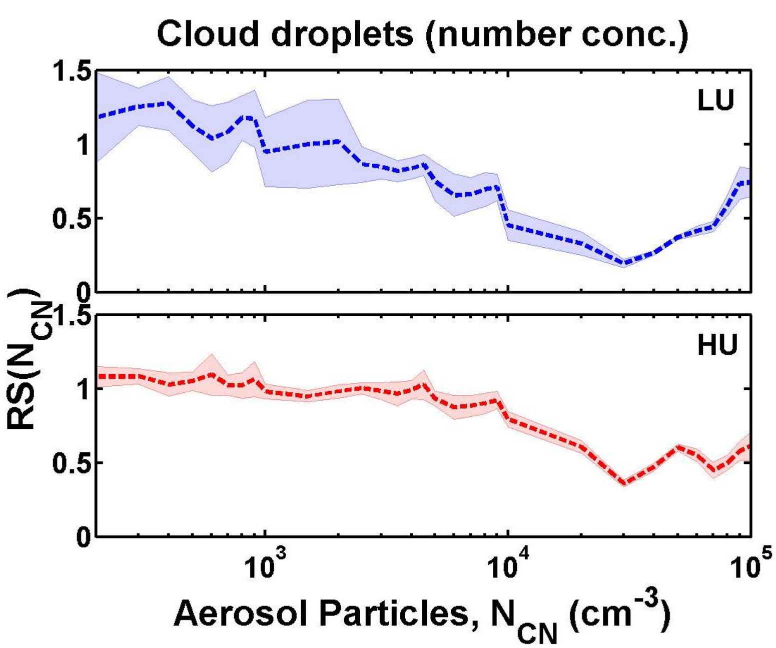

Cloud droplets (number conc.)
LU
HU
RS(N_{CN})
Aerosol Particles, N_{CN} (cm^{-3})
1.5
1
0.5
0
10^3
10^4
10^5

(c)

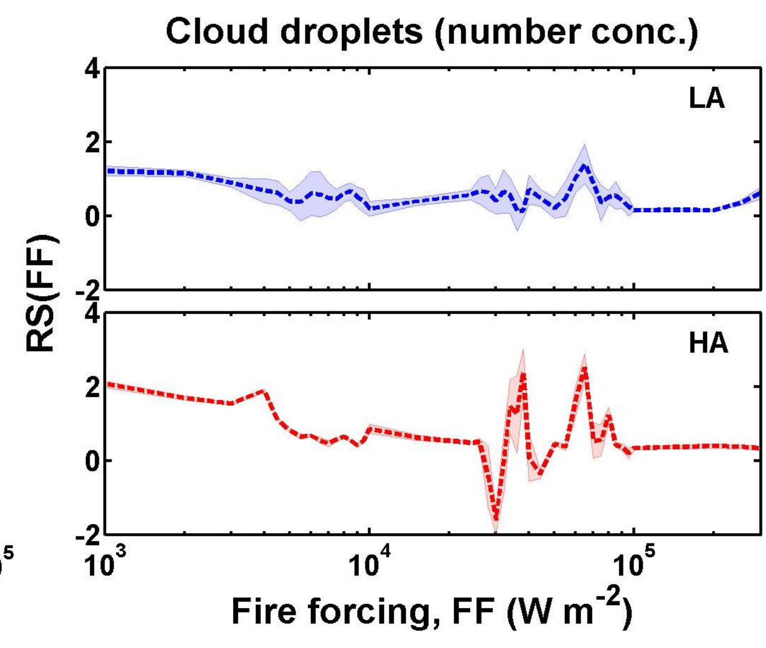

Cloud droplets (number conc.)
LA
HA
RS(FF)
Fire forcing, FF (W m^{-2})
4
2
0
-2
10^3
10^4
10^5

(d)

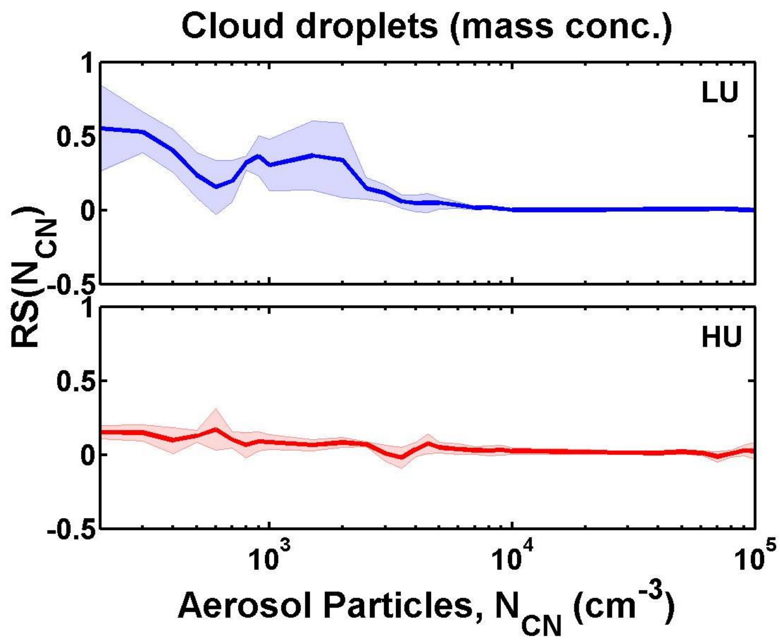

(e)

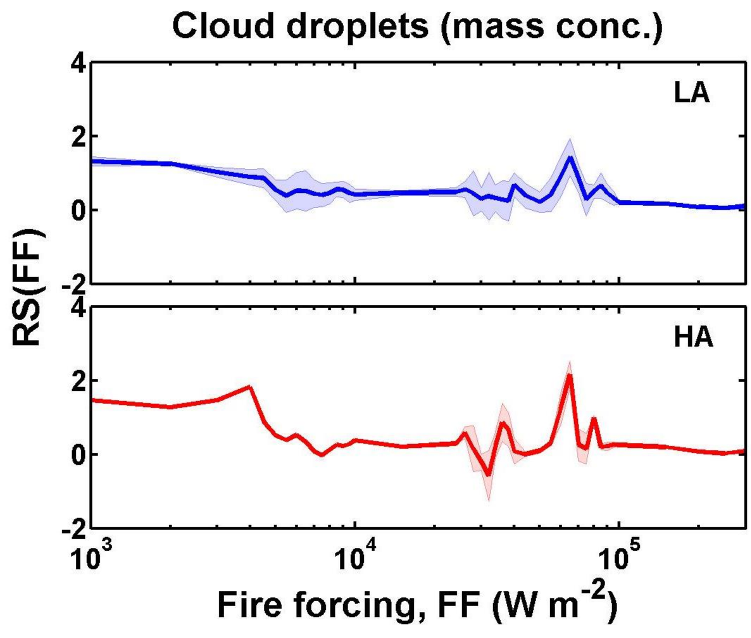

(f)

Figure 7. Number (a) and mass concentration (b) of cloud droplets calculated as a function of aerosol number concentration (N_{CN}) and updraft velocity (represented by *FF*). Red dashed lines indicate the borders between different regimes defined by $RS\ (N_{\mathrm{CN}})/RS(FF)$=4 or 1/4, respectively. Relative sensitivities with respect to N_{CN} (left) and *FF* (right) for number (panels (c) and (d)) and mass (panels (e) and (f)) concentration of cloud droplets under different conditions. The thick dashed or solid lines represent the mean values under a given condition, and the shaded areas represent the variability of estimation (±½σ). The acronyms indicate LU: low updrafts (1,000–7,000 W m^{-2}); HU: high updrafts (75,000–300,000 W m^{-2}); LA: low aerosols (200–1,500 cm^{-3}); HA: high aerosols (10,000–100,000 cm^{-3}).

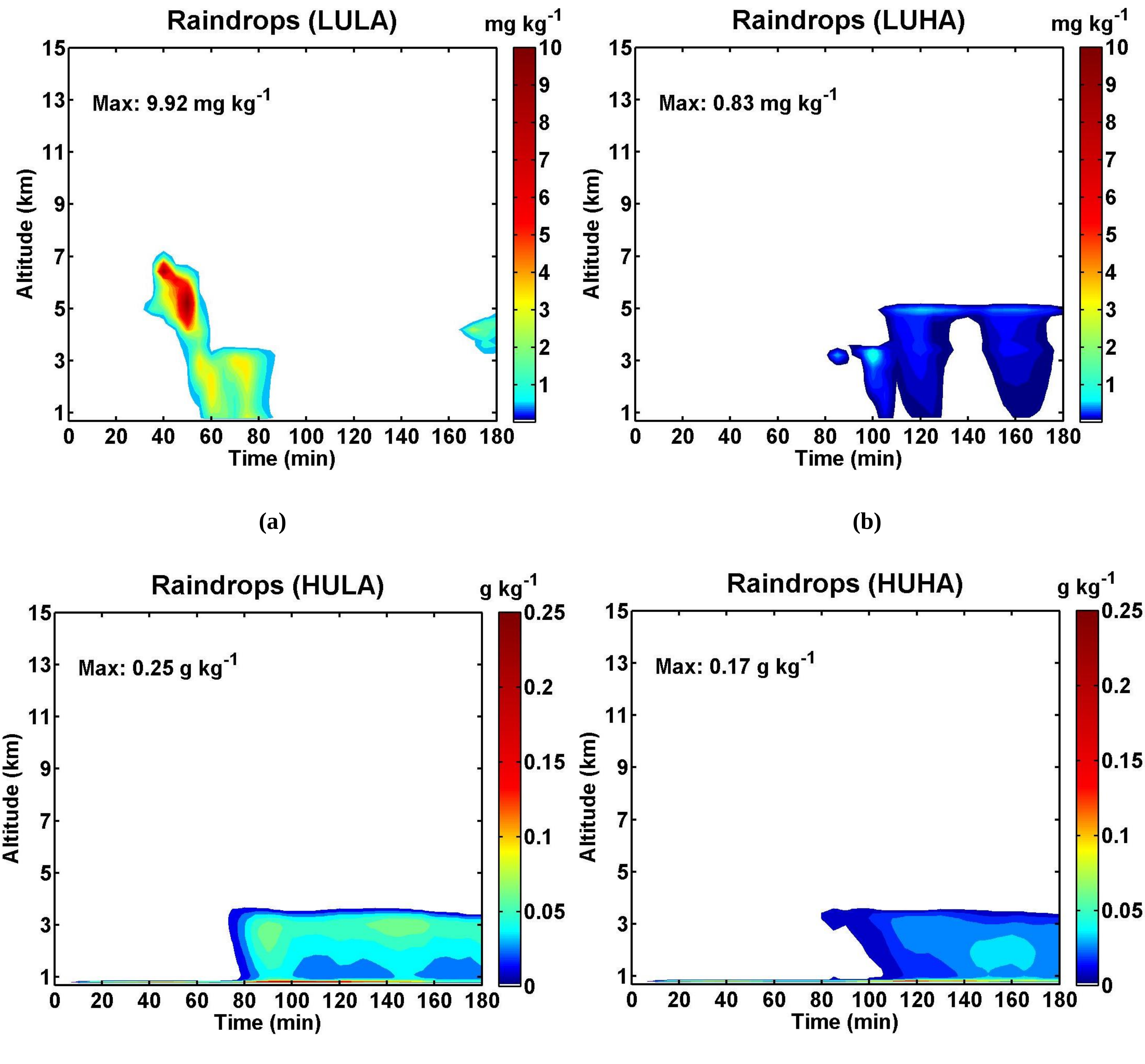

Figure 8. Same as Figure 6 but for raindrops.

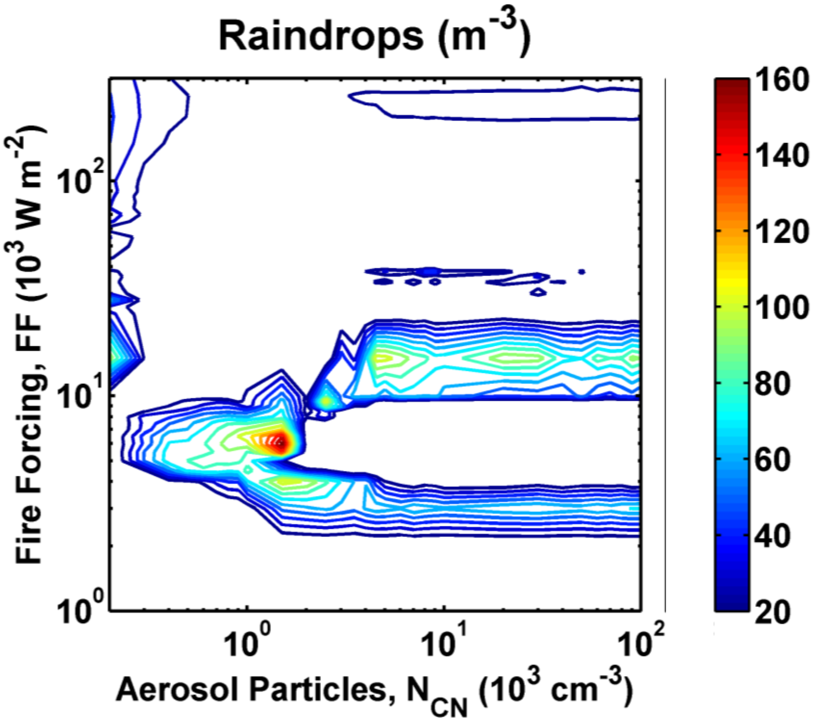
Raindrops (m^{-3})
Fire Forcing, FF (10^3 W m^{-2})
Aerosol Particles, N_{CN} (10^3 cm^{-3})
160
140
120
100
80
60
40
20

(a)

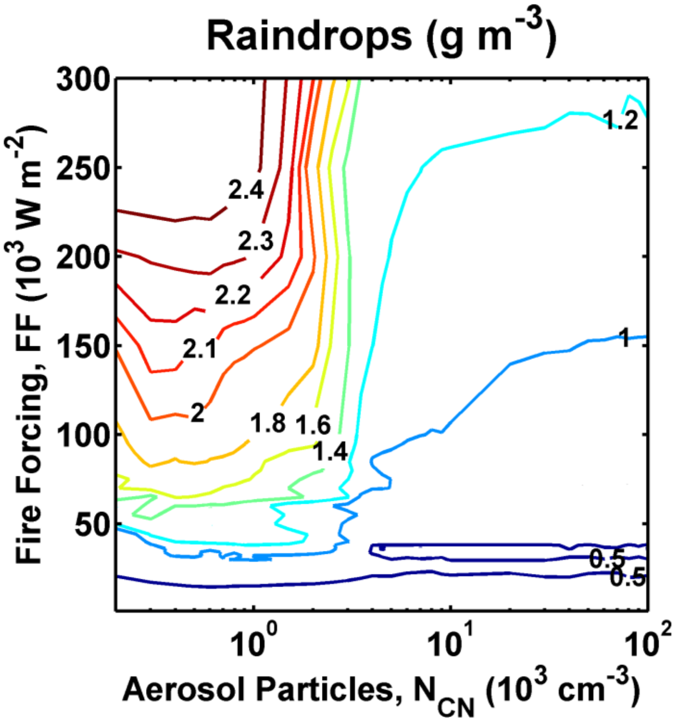
Raindrops (g m^{-3})
Fire Forcing, FF (10^3 W m^{-2})
Aerosol Particles, N_{CN} (10^3 cm^{-3})
2.4
2.3
2.2
2.1
2
1.8
1.6
1.4
1.2
1
0.5
0.5

(b)

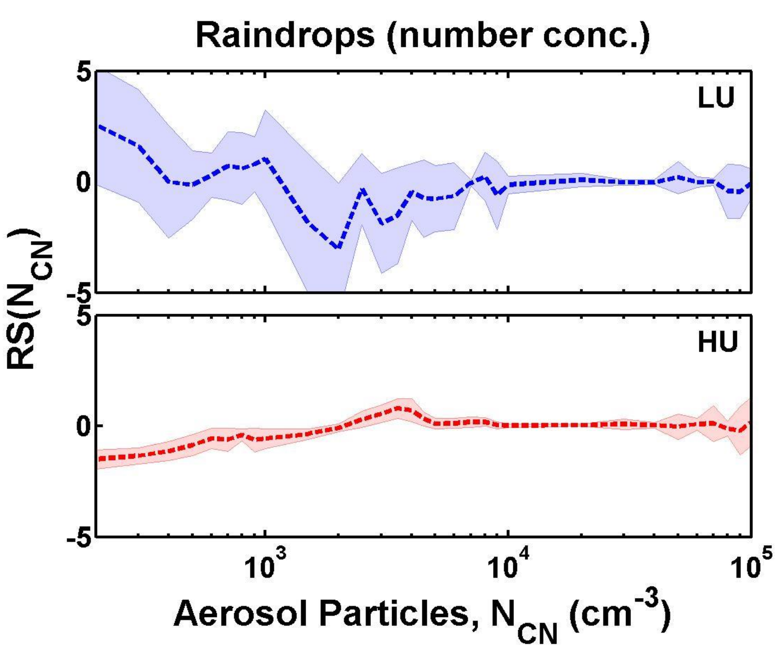
Raindrops (number conc.)
LU
HU
RS(N_{CN})
Aerosol Particles, N_{CN} (cm^{-3})

(c)

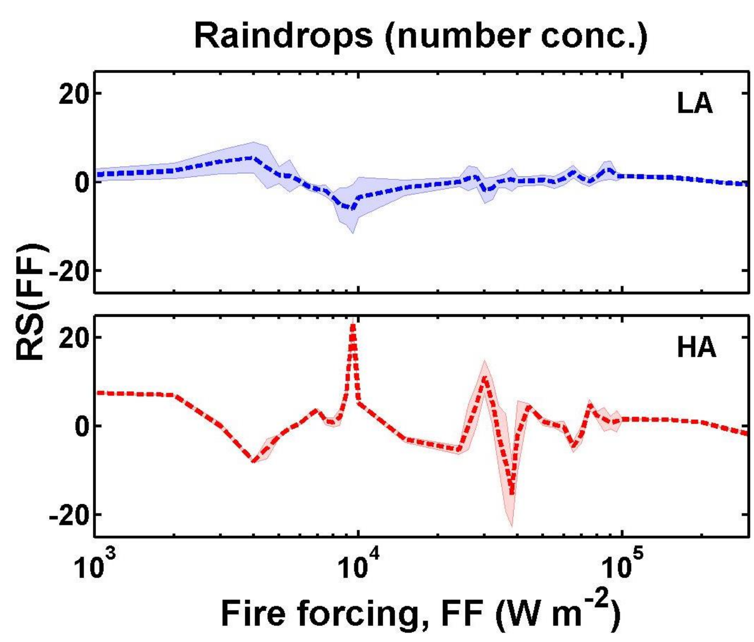
Raindrops (number conc.)
LA
HA
RS(FF)
Fire forcing, FF (W m^{-2})

(d)

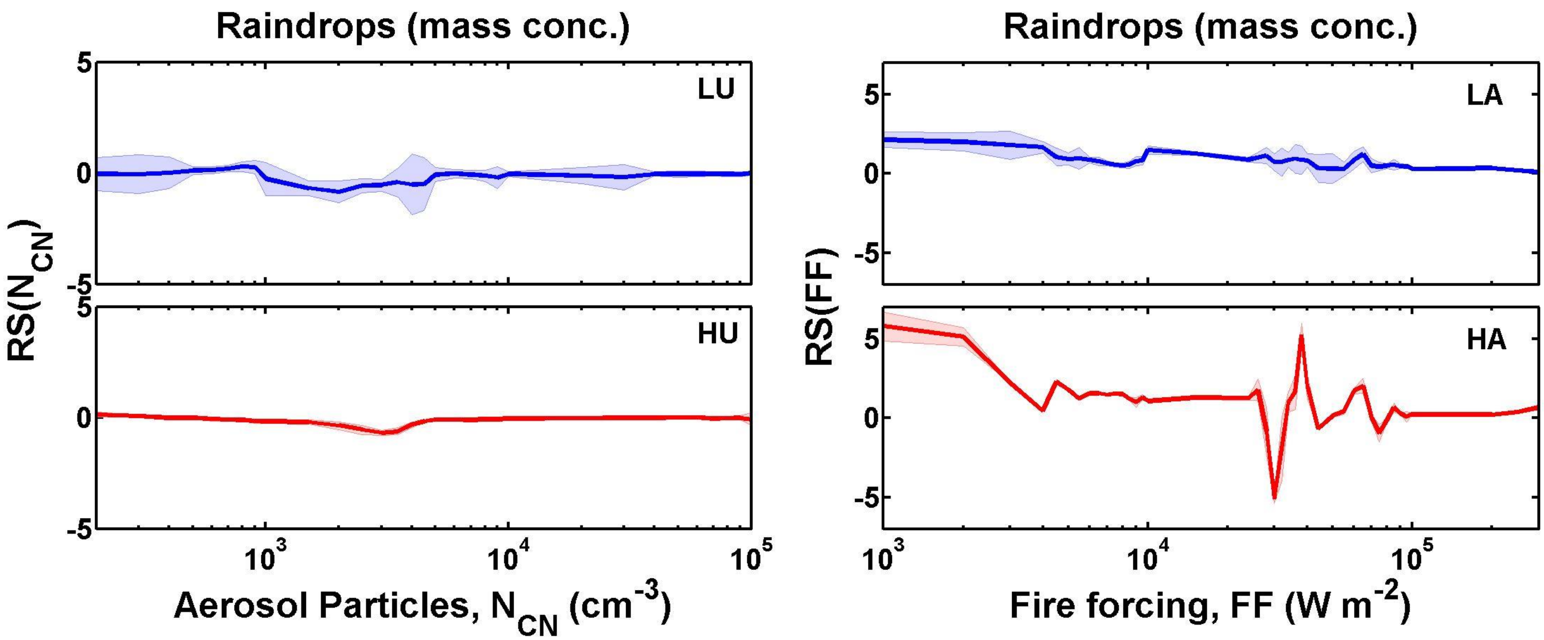

(e) **(f)**

Figure 9. Same as Figure 7 but for raindrops.

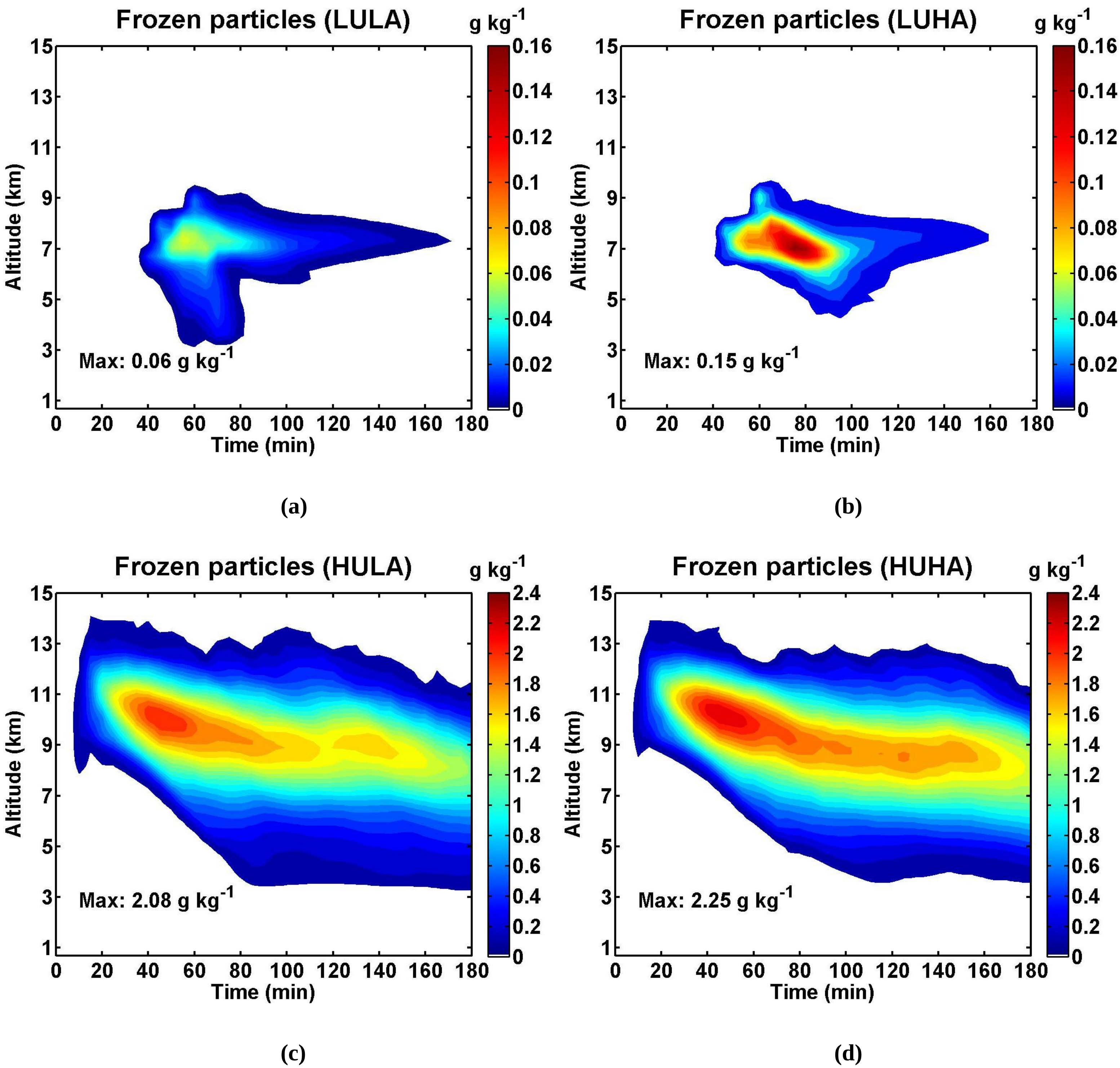

Figure 10. Same as Figure 6 but for the frozen particles.

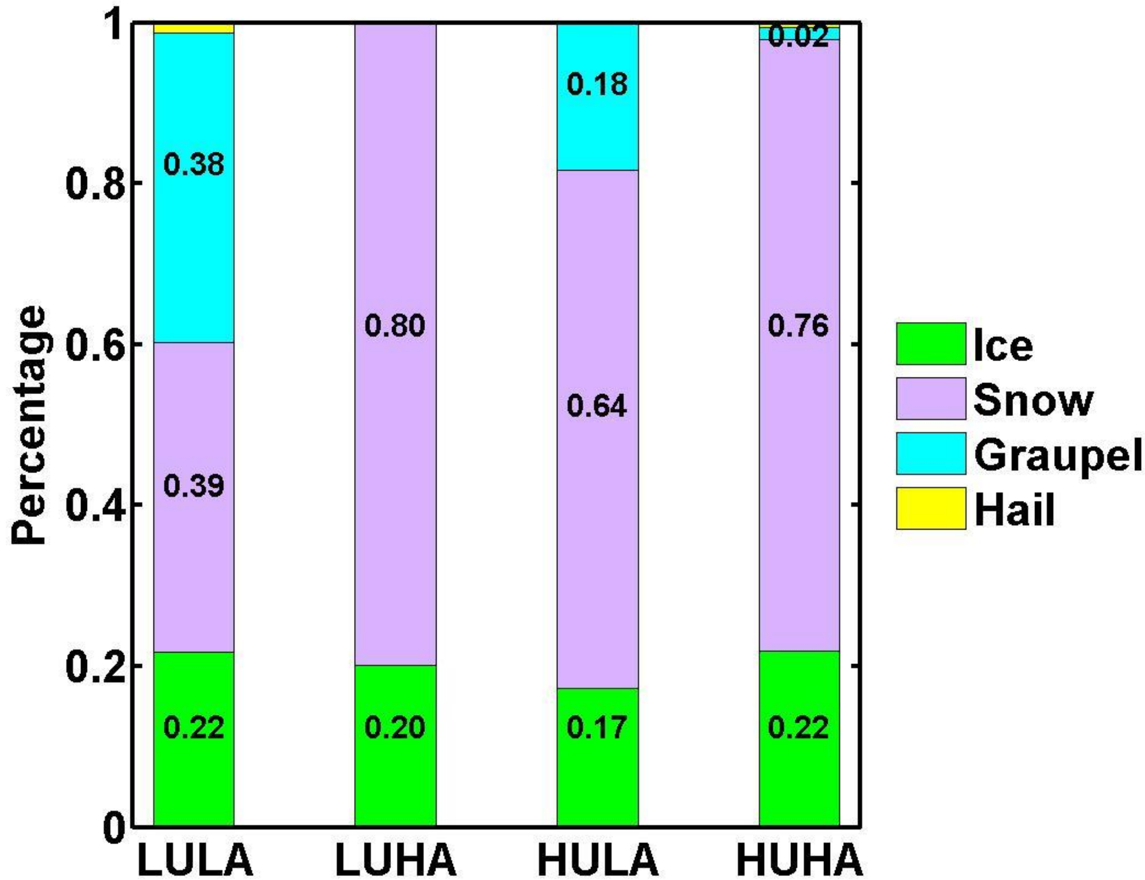

Figure 11. Contributions of individual frozen hydrometeor to total frozen water content under four extreme conditions which are referred to as (1) LULA: low updrafts (2,000 W m^{-2}) and low aerosols (200 cm^{-3}); (2) LUHA: low updrafts (2,000 W m^{-2}) and high aerosols (100,000 cm^{-3}); (3) HULA: high updrafts (300,000 W m^{-2}) and low aerosols (200 cm^{-3}); (4) HUHA: high updrafts (300,000 W m^{-2}) and high aerosols (100,000 cm^{-3}).

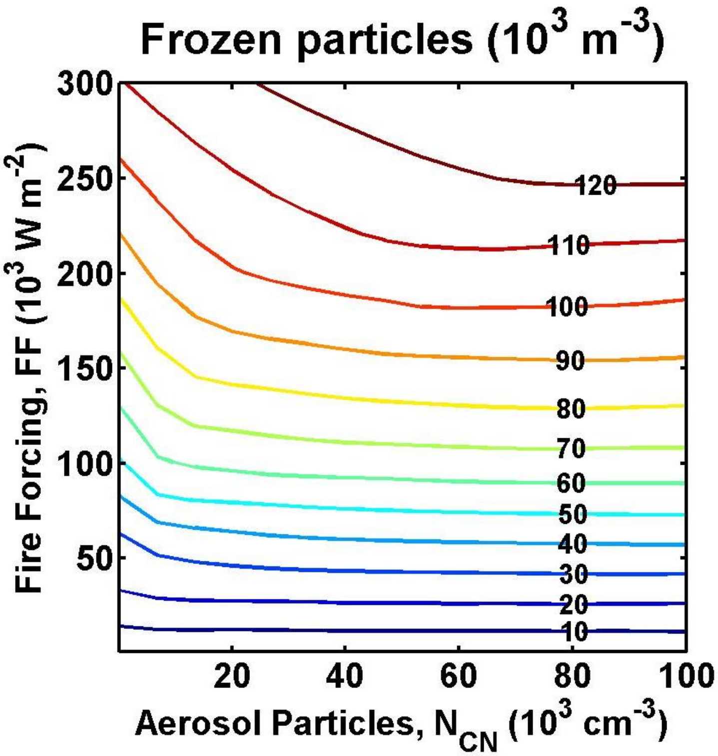
Frozen particles (10^3 m^-3)
Fire Forcing, FF (10^3 W m^-2)
Aerosol Particles, N_CN (10^3 cm^-3)
300
250
200
150
100
50
20
40
60
80
100
120
110
100
90
80
70
60
50
40
30
20
10

(a)

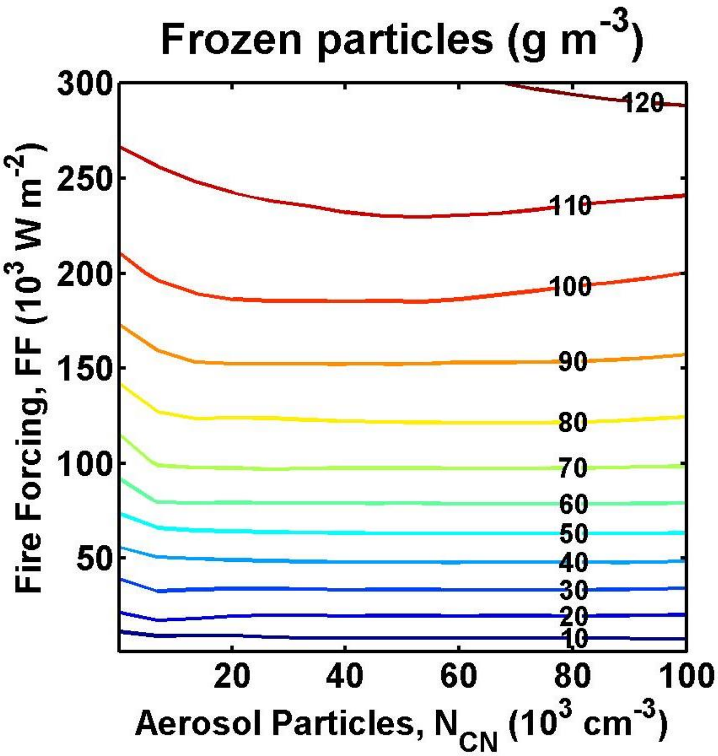
Frozen particles (g m^-3)
Fire Forcing, FF (10^3 W m^-2)
Aerosol Particles, N_CN (10^3 cm^-3)
300
250
200
150
100
50
20
40
60
80
100
120
110
100
90
80
70
60
50
40
30
20
10

(b)

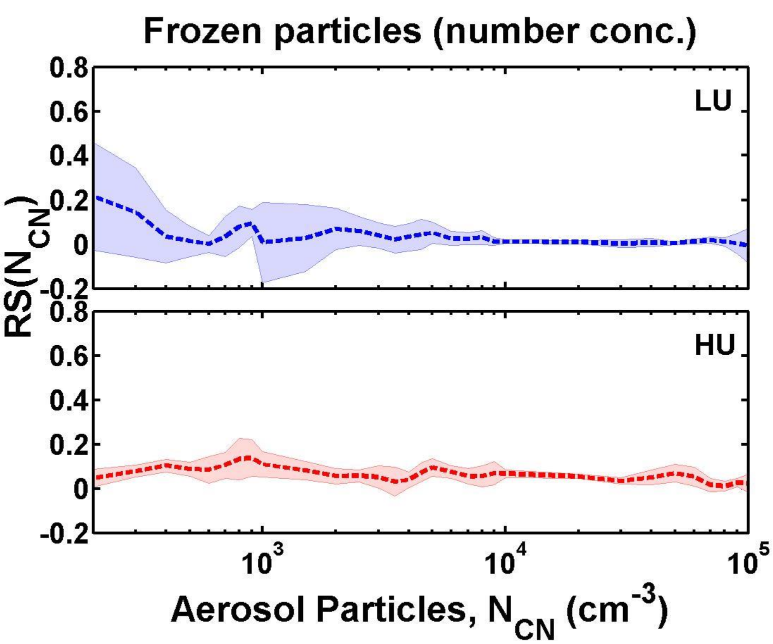
Frozen particles (number conc.)
RS(N_CN)
Aerosol Particles, N_CN (cm^-3)
LU
HU
0.8
0.6
0.4
0.2
0
-0.2
10^3
10^4
10^5

(c)

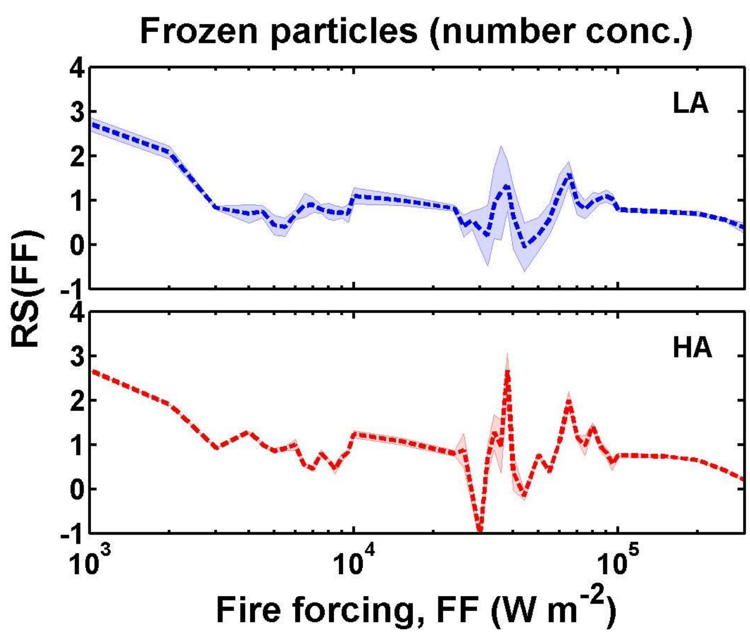
Frozen particles (number conc.)
RS(FF)
Fire forcing, FF (W m^-2)
LA
HA
4
3
2
1
0
-1
10^3
10^4
10^5

(d)

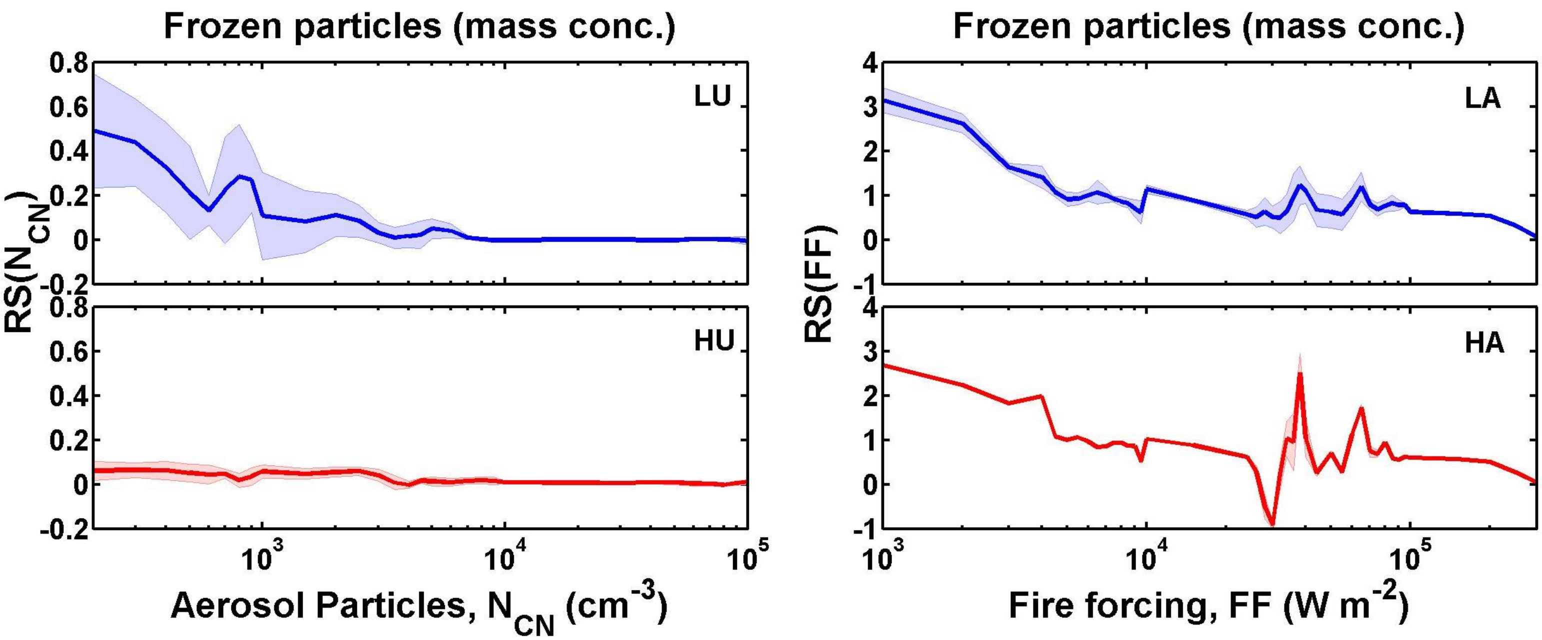

(e) **(f)**

Figure 12. Same as Figure **7** but for total frozen particles.

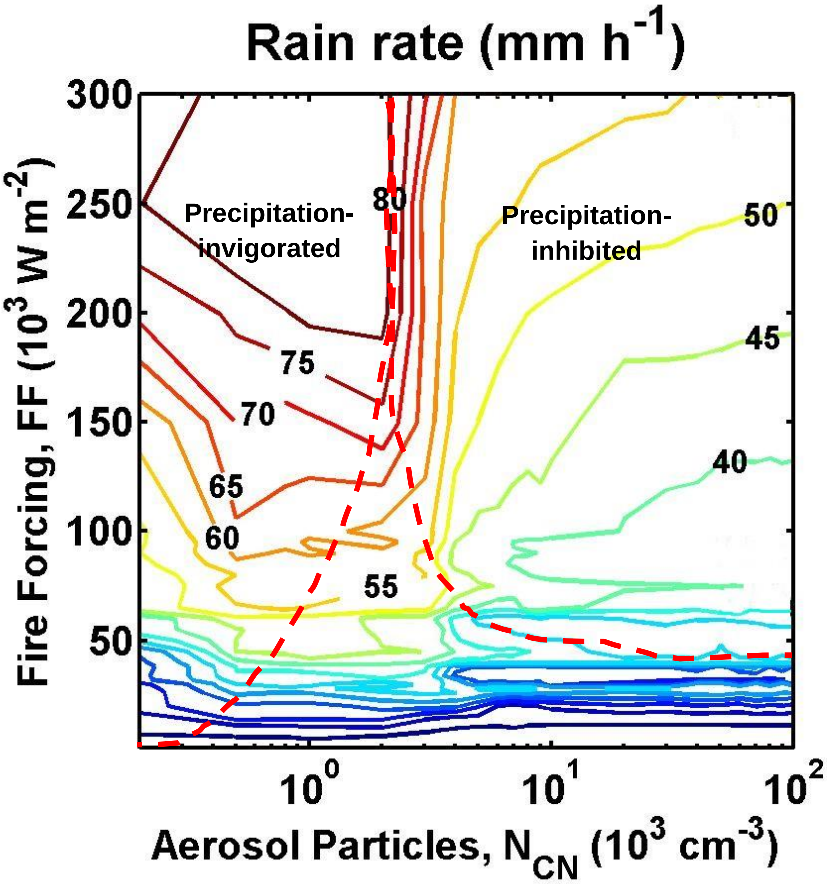

(a)

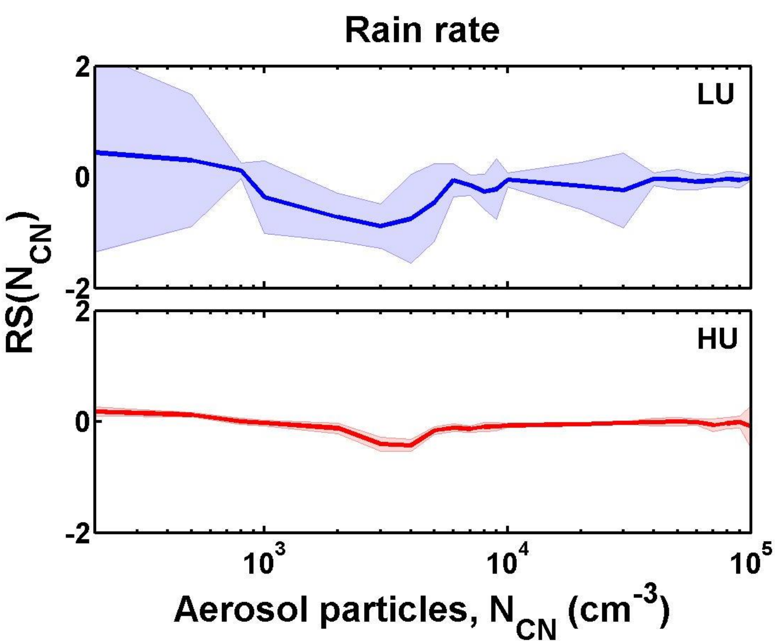

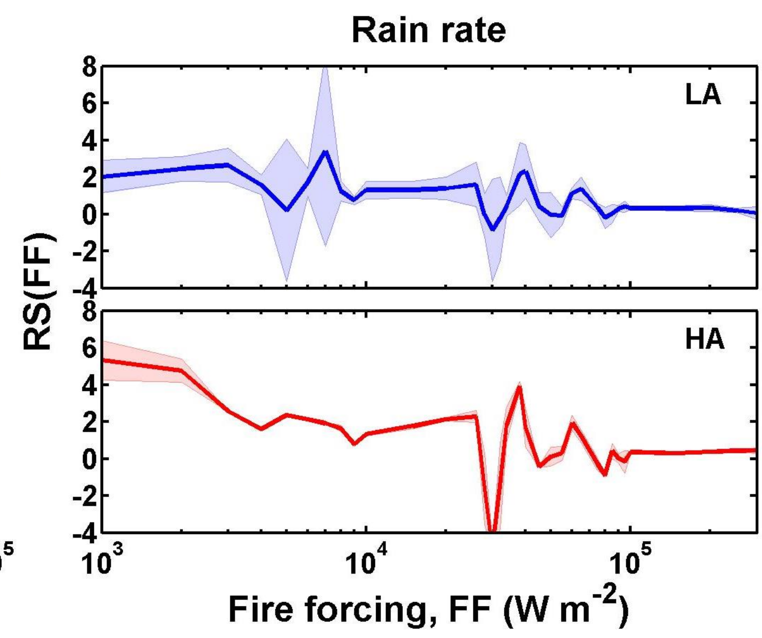

(b) **(c)**

Figure 13. Same as Figure 7 but for surface rain rate.

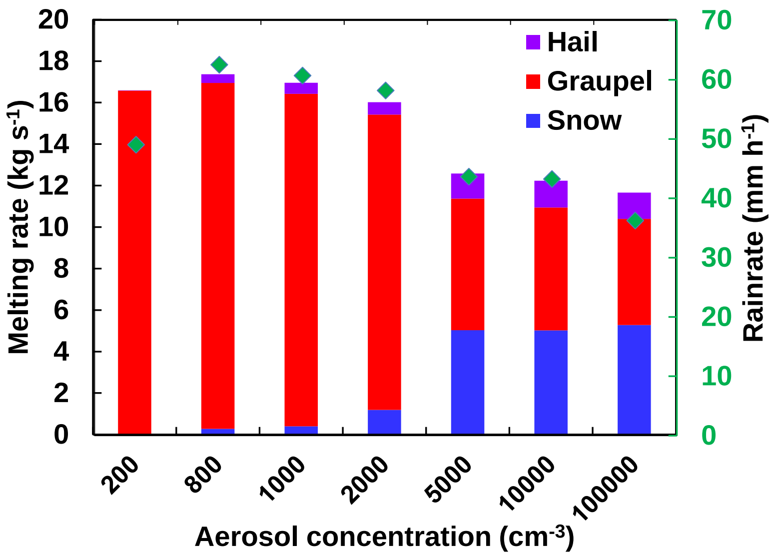

Figure 14. The correlation of rain rate and the melting rate of the frozen particles. The green diamond points are the averaged rain rate under different aerosol concentrations (*FF*= 10^5 W m^{-2}). The columns represent the integrated melting rate from individual frozen particles.

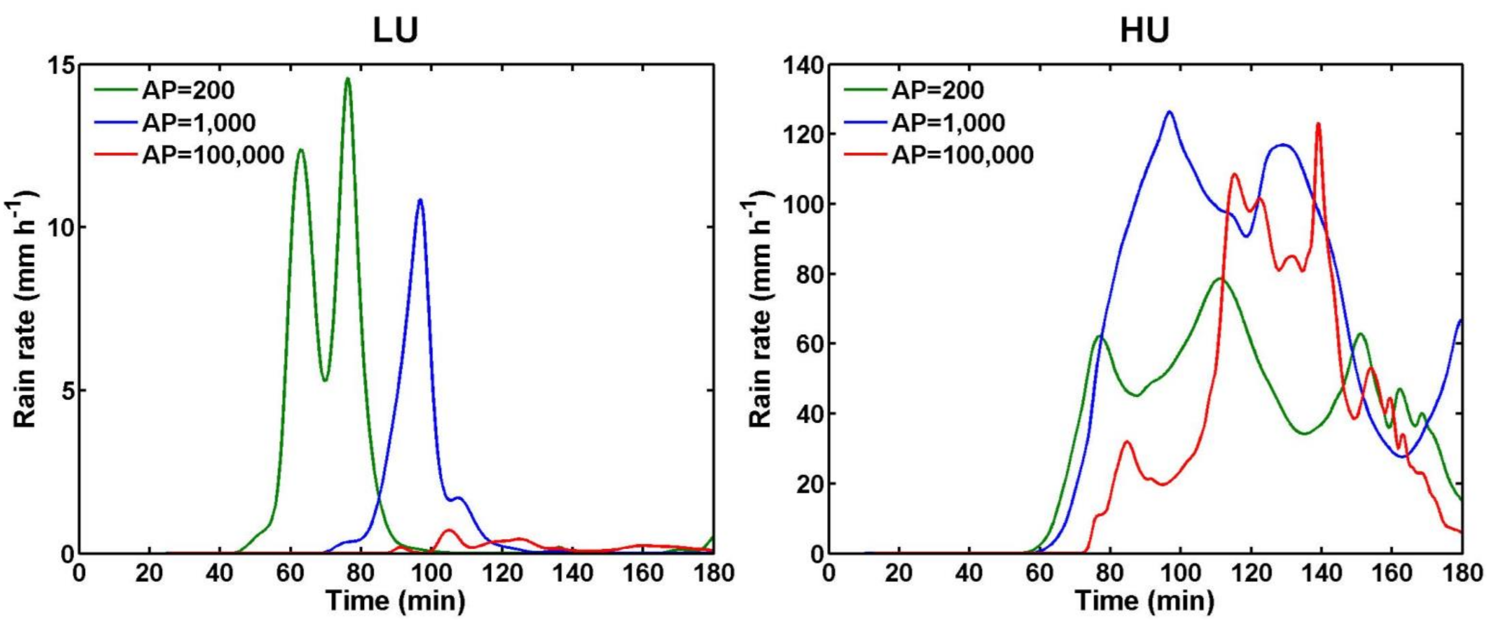

Figure 15. Time evolution of surface rain rates for the three aerosol episodes (N_{CN} = 200; 1,000; and 100,000 cm^{-3} respectively) under LU (low updrafts, *FF*=2,000 W m^{-2}) and HU (high updrafts, *FF*=50,000 W m^{-2}) conditions.

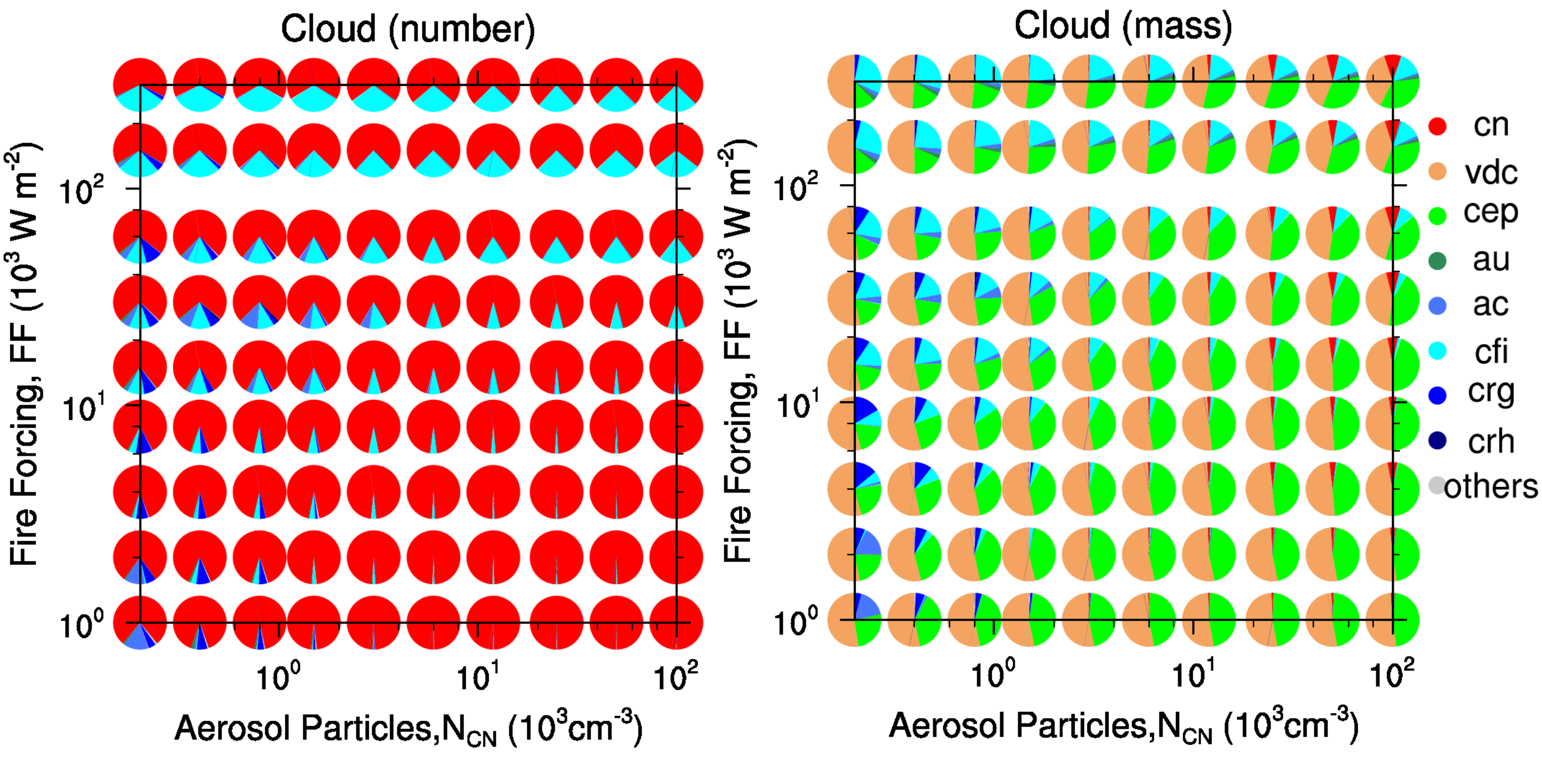

(a)

(b)

Figure 16. The pie charts summarize the relative percentage of the microphysical processes involving cloud droplets as a function of N_{CN} and fire forcing (a: number concentration; b: mass concentration). Colors within each pie chart reflect the contribution of processes under the specific condition. Warm colors denote the sources, while cold colors denote the sinks. The acronyms indicate cn: cloud nucleation; vdc: condensational growth of cloud droplets; cep: evaporation of cloud droplets; au: autoconversion; ac: accretion; cfi: freezing of cloud droplets to form ice crystals, including homogeneous and heterogeneous nucleation; crg/h: riming of cloud droplets to form graupel/hail.

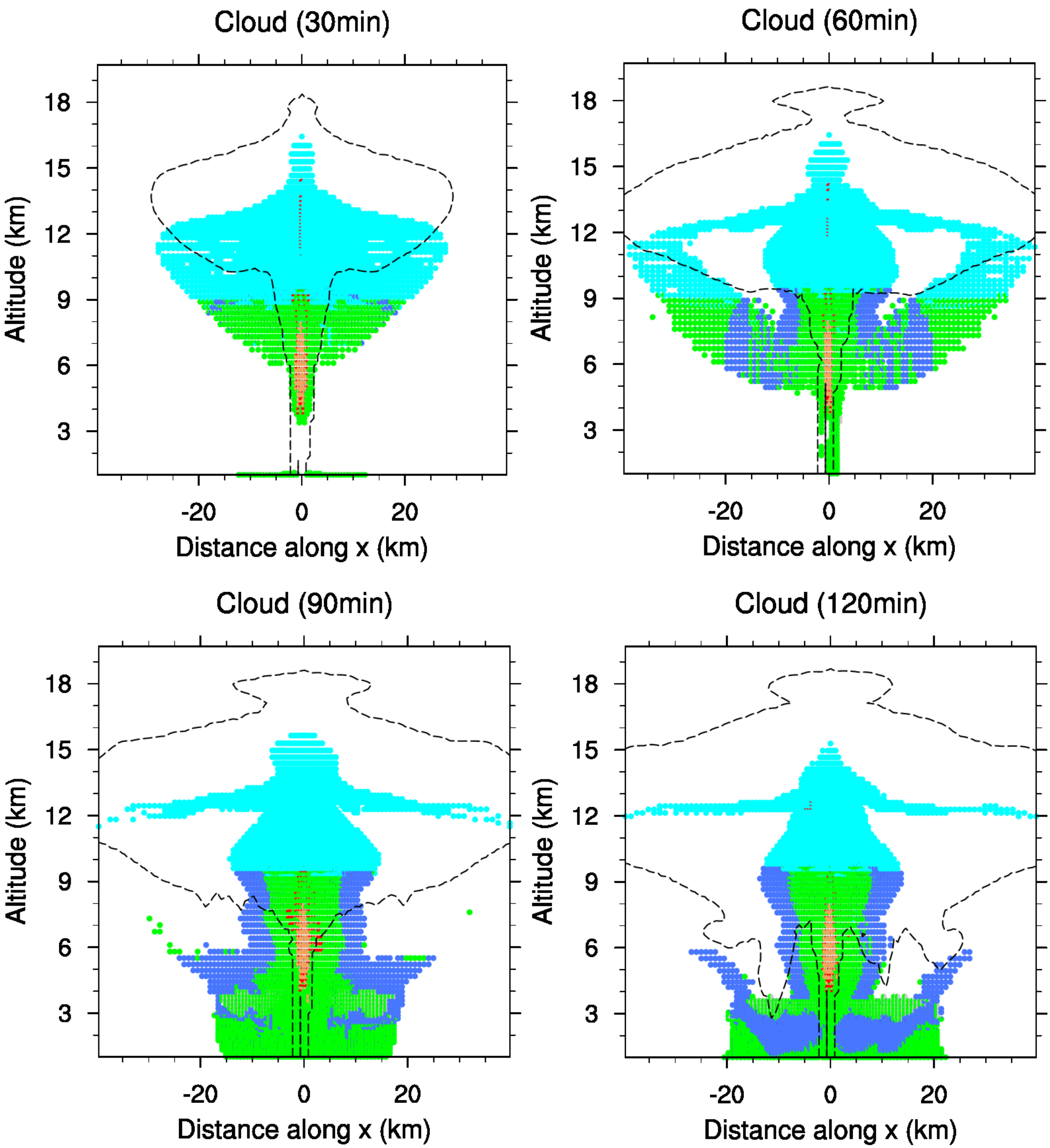
Cloud (30min)
Cloud (60min)
Cloud (90min)
Cloud (120min)
Altitude (km)
18
15
12
9
6
3
-20
0
20
Distance along x (km)

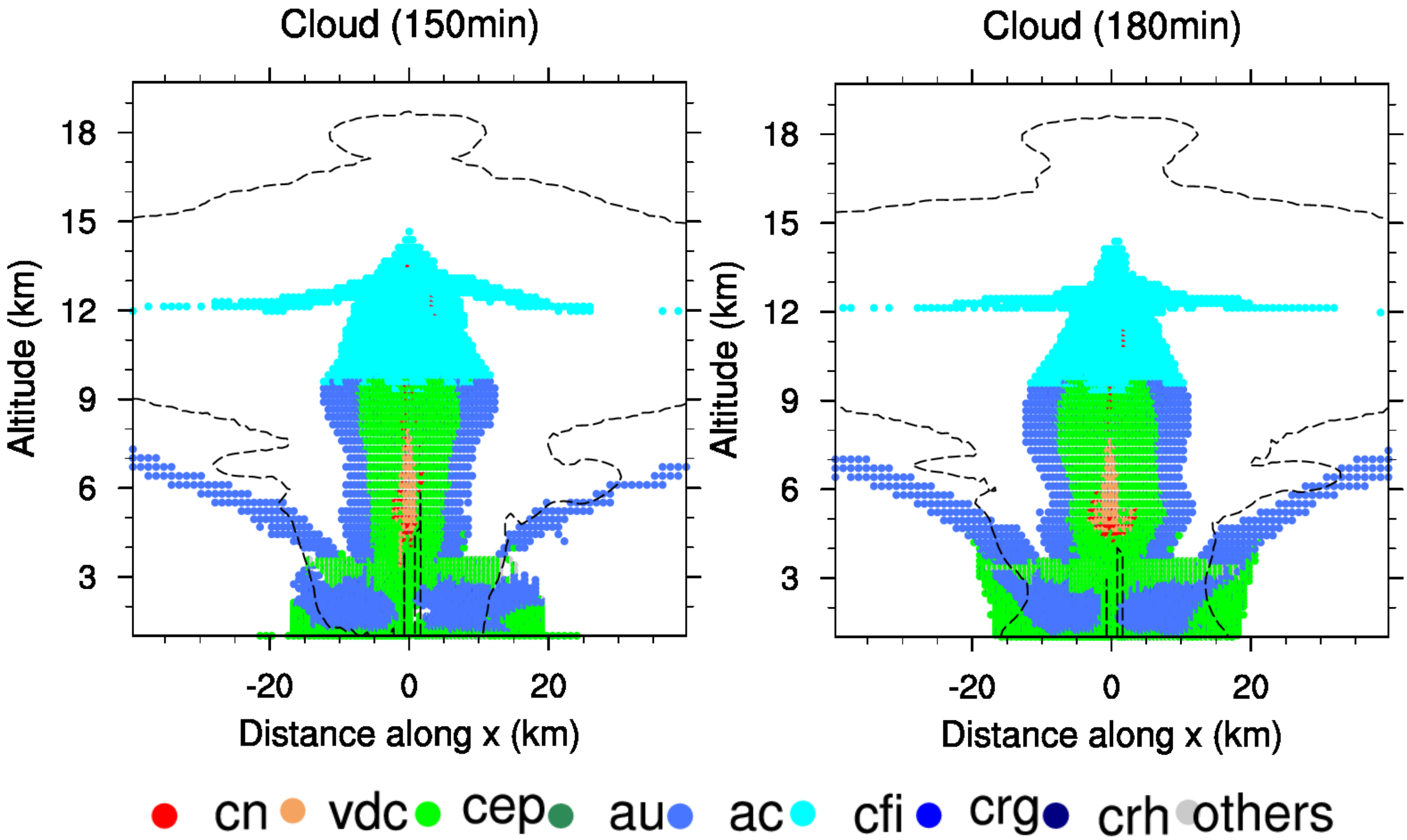

Figure 17. The pie charts summarize the vertical cross sections of the change rate of main microphysical processes contributing to cloud water content. Each pie chart shows the averaged contribution over the past 30 min. Colors within each pie chart reflect the percentage of processes in each grid. The black dashed line is the 0.1 μg kg^{-1} isoline of the interstitial aerosol, indicating the shape of smoke plume. The meaning of the acronyms is the same as in Figure 16. Warm colors denote the sources, while cold colors denote the sinks.

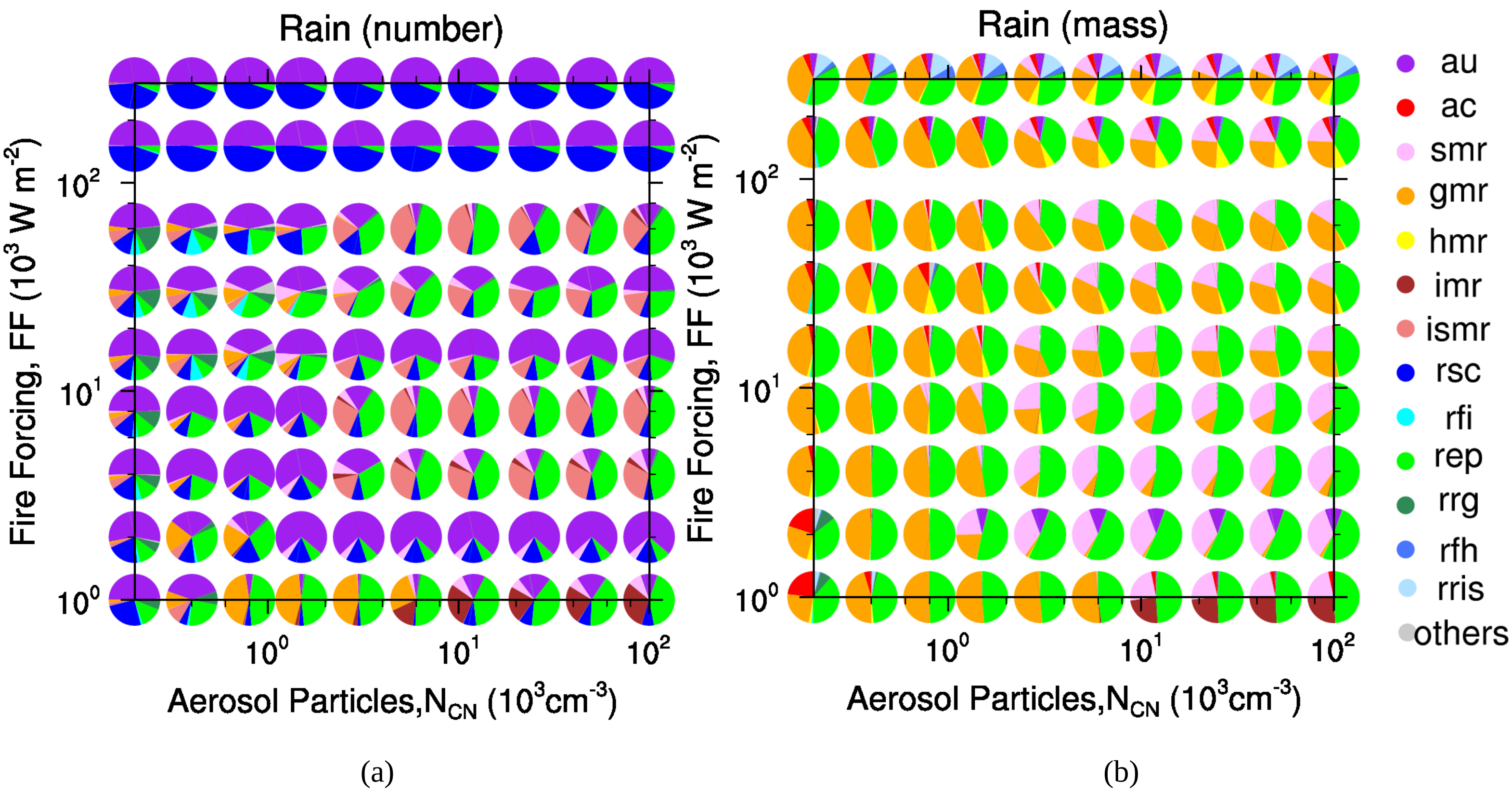

(a) (b)

Figure 18. Same as Figure 16 but for raindrops. The acronyms indicate au: autoconversion; ac: accretion; i/s/g/hmr: melting of ice/snow/graupel/hail to form raindrops; rsc: self-collection of raindrops; ismr: melting of ice and snow to form raindrops; rfi/h: freezing of raindrops to form ice crystals/hail; rep: raindrop evaporation; rrg: riming of raindrops to form graupel; rris: riming of raindrops to form ice and snow.

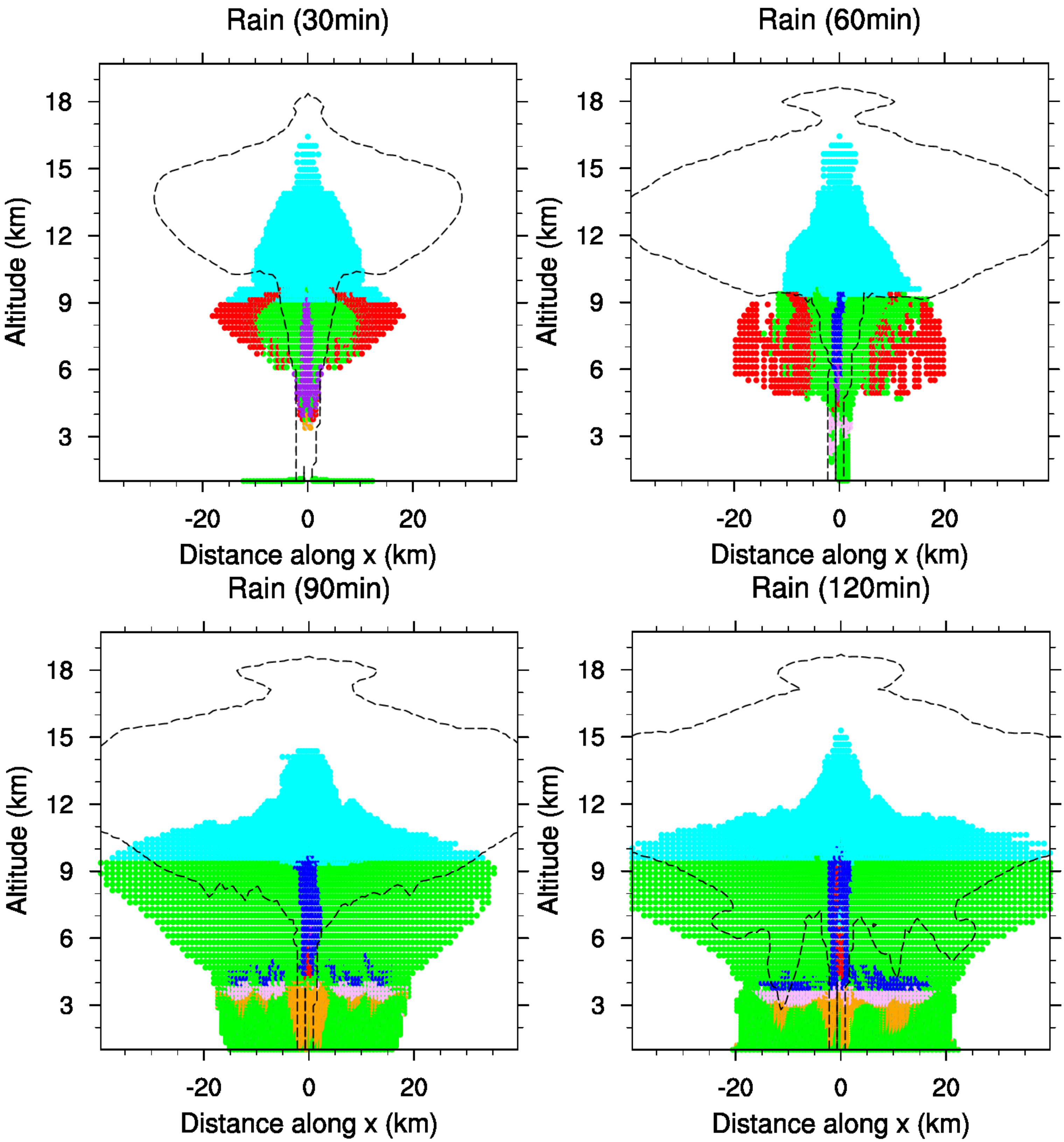

Rain (30min)
Rain (60min)
Rain (90min)
Rain (120min)
Altitude (km)
Distance along x (km)
18
15
12
9
6
3
-20
0
20

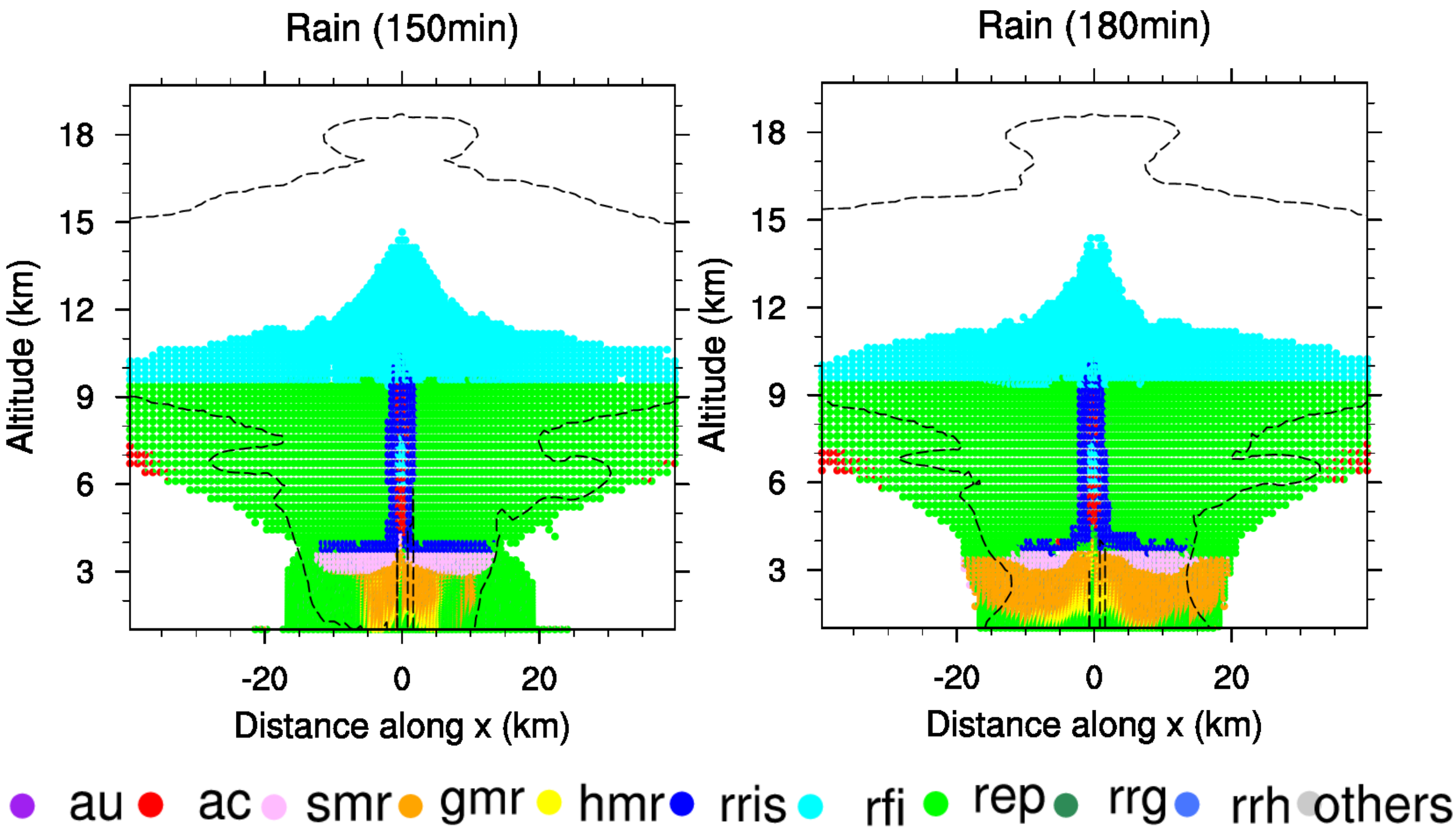

Figure 19. Same as Figure 17, but for raindrops.

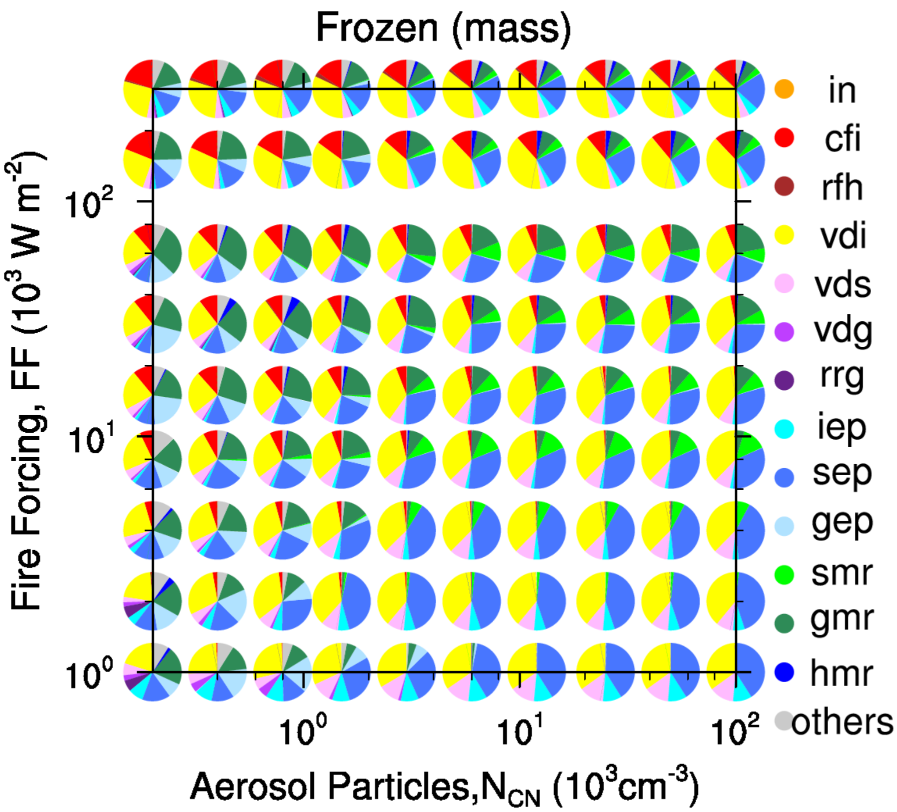

Figure 20. Same as Figure 16 but for the total frozen water content. The acronyms indicate in: ice nucleation; cfi: freezing of cloud droplets to form ice crystals, including homogeneous and heterogeneous nucleation; rfh: freezing of raindrops to form hail; vdi/s/g: condensational growth of ice crystals/snow/graupel by water vapor; rrg: riming of raindrops to form graupel; i/s/gep: evaporation of ice/snow/graupel; s/g/hmr: melting of snow/graupel/hail to form raindrops.

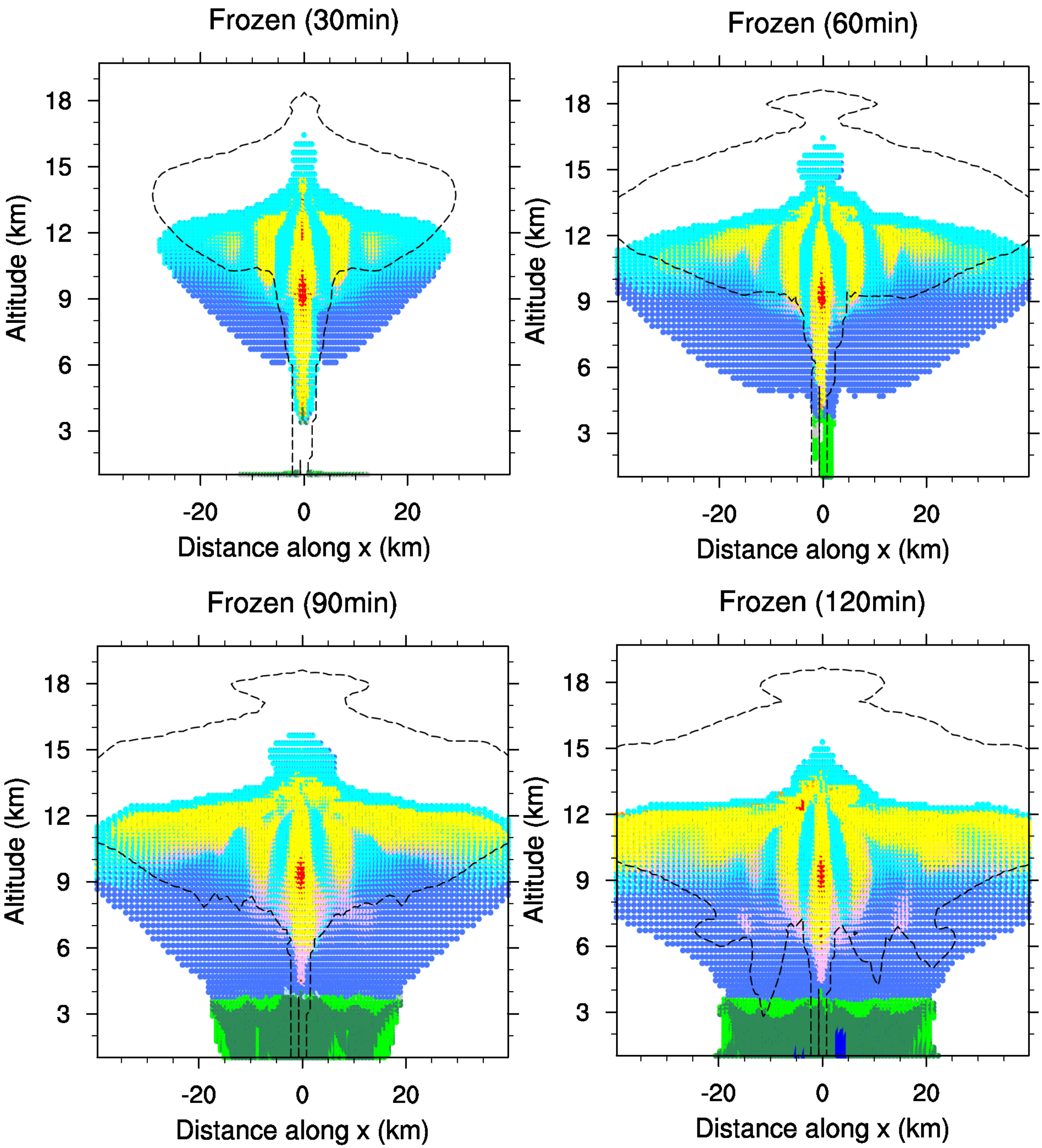
Frozen (30min)
Frozen (60min)
Frozen (90min)
Frozen (120min)
Altitude (km)
Distance along x (km)
18
15
12
9
6
3
-20
0
20

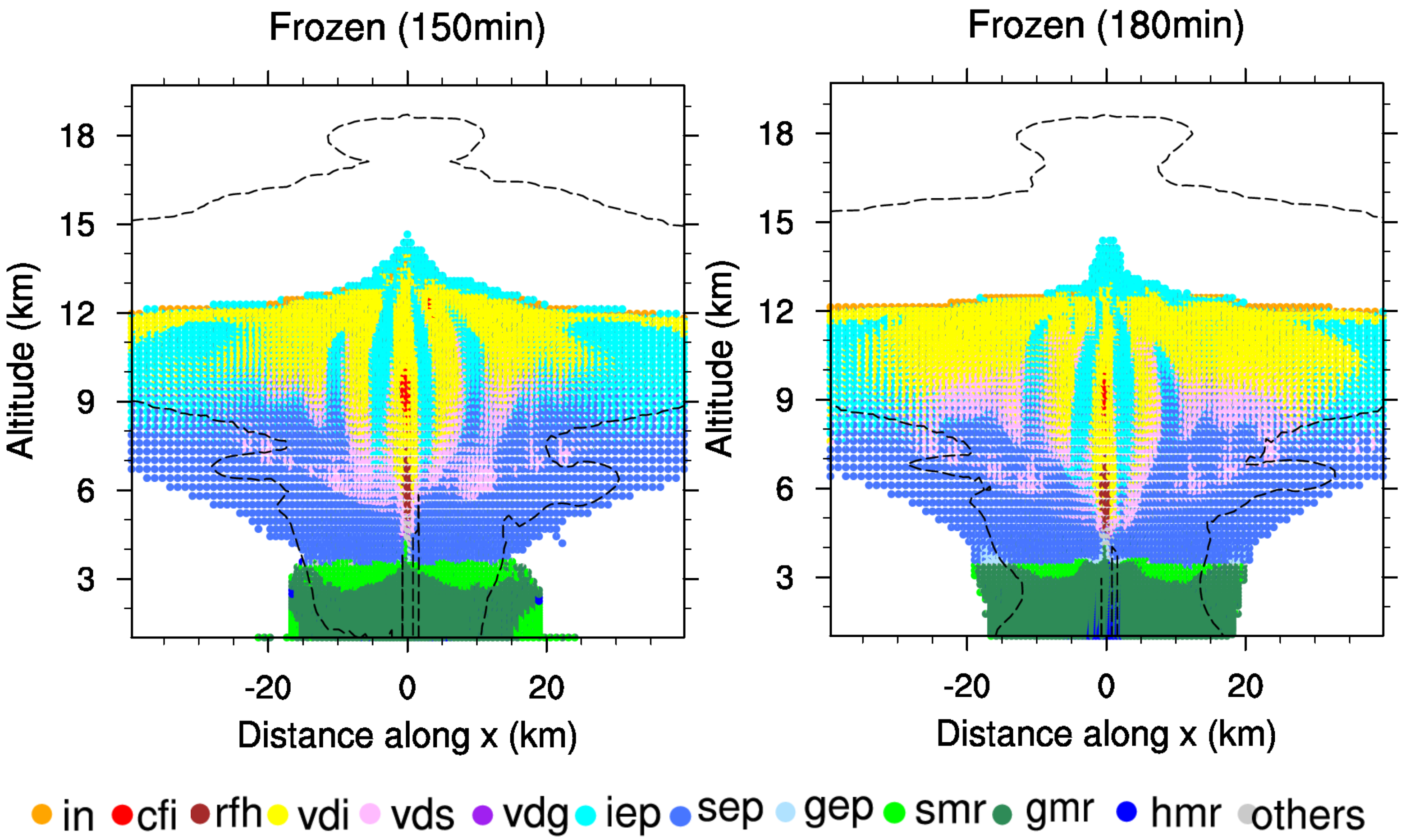

Figure 21. Same as Figure 17 but for frozen particles.

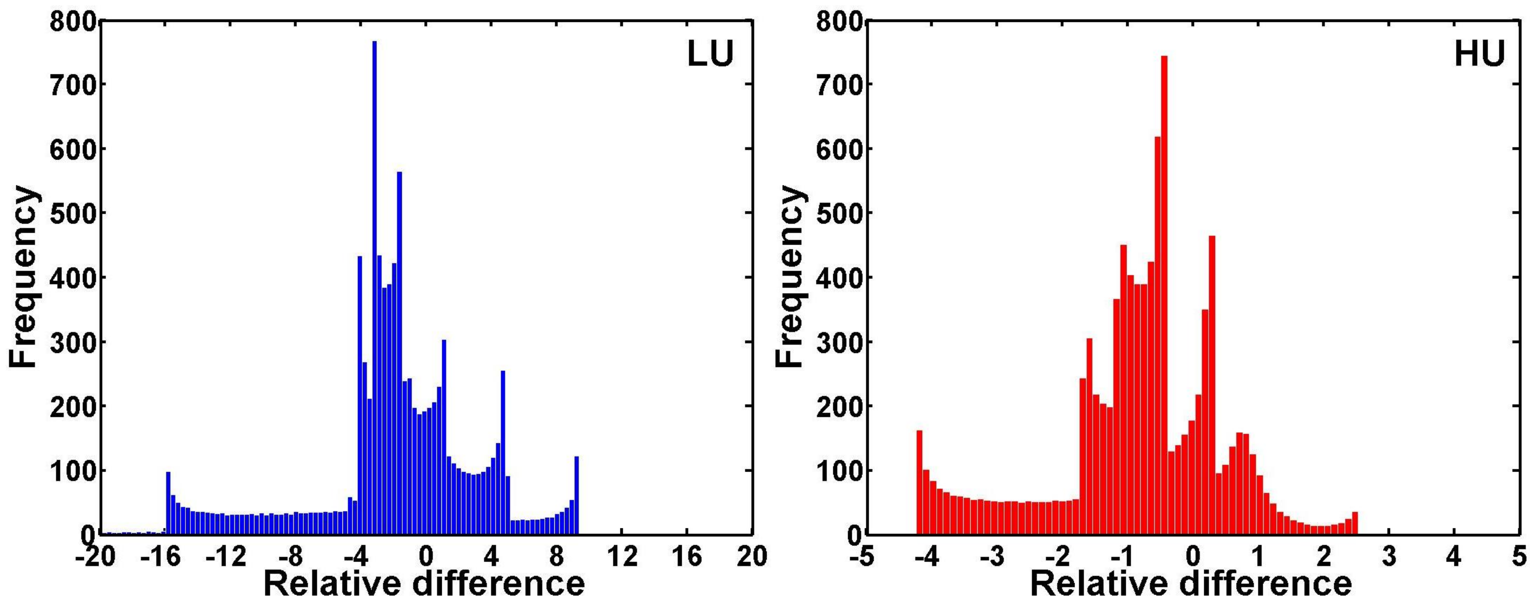

Figure 22. Histograms of the relative difference between $\frac{\Delta Y}{\Delta N_{CN}}$ and $\frac{dY}{dN_{CN}}$ under LU and HU conditions, where Y here denotes precipitation rate. $\frac{\Delta Y}{\Delta N_{CN}} = \frac{Y(2N_{CN}) - Y(N_{CN})}{2N_{CN} - N_{CN}}$, and $\frac{dY}{dN_{CN}}$ is the derivative of the precipitation rate along the variable N_{CN}.

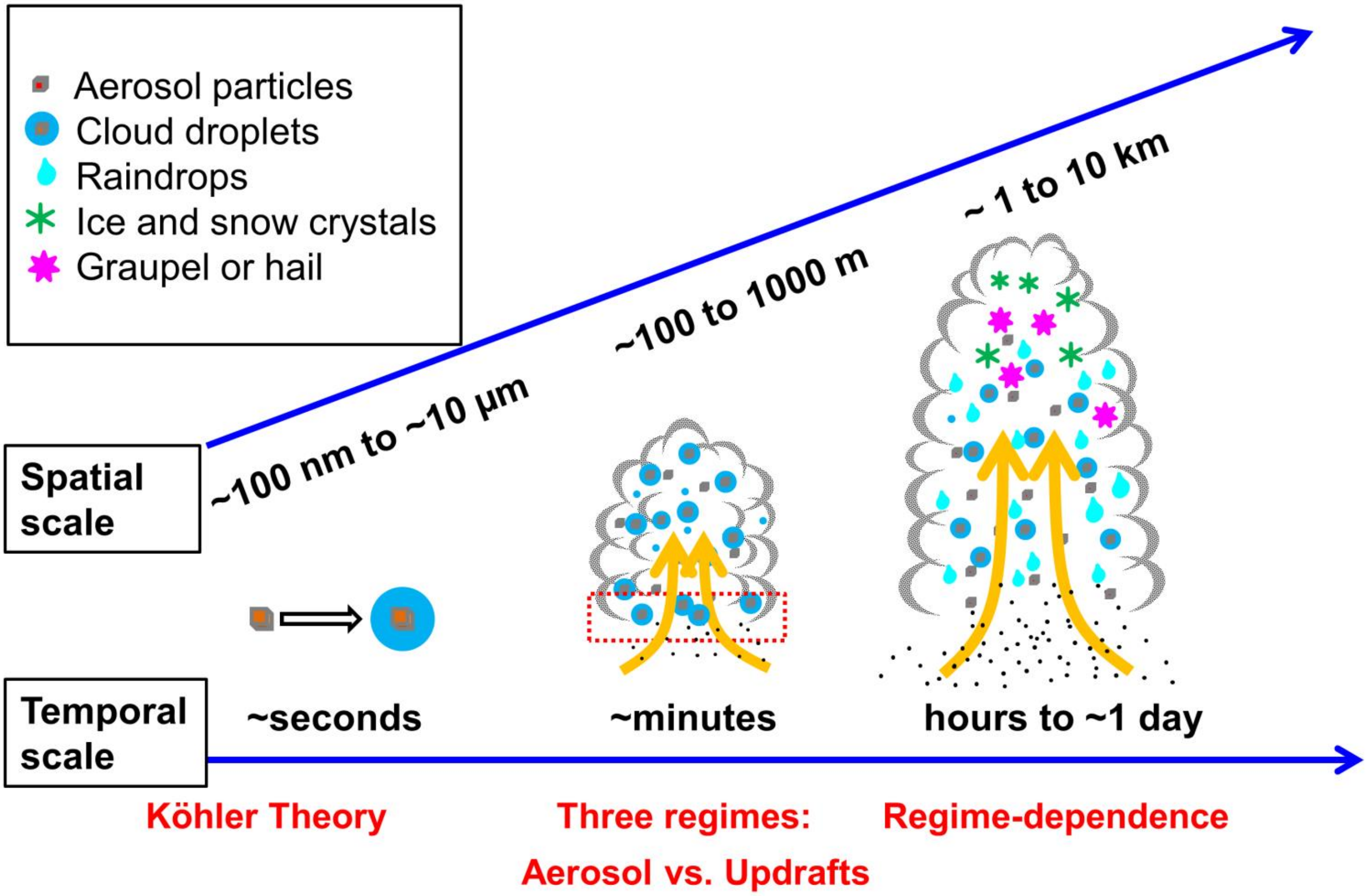

Figure 23. Overview of the research approaches on multi-scale cloud initialization and development. The aerosol-cloud interaction at the microphysical scale, i.e., cloud condensation nuclei (CCN) activation, has been well characterized by the Köhler theory (Kohler, 1936) and by a series of extended equations (Shulman et al., 1996; Kulmala et al., 1997; Laaksonen et al., 1998). When we upscale the activation of a single aerosol particle to aerosol populations at the cloud base, the impact of aerosols on the number of activated CCN still appears simple and can be well described (i.e., the three generic regimes of CCN activation). When considering full microphysics and the larger temporal and spatial scales of a single pyro-convective cloud, the performance of ensemble simulations shows the regime dependence of aerosol effects on the pyro-convective cloud formation and evolution.